Assessing materials quality for high efficiency electricity generation

by

Eveline Postelnicu

Submitted to the
Department of Materials Science and Engineering
in Partial Fulfillment of the Requirements for the Degree of

Bachelor of Science

at the

Massachusetts Institute of Technology

June 2017

Signature of author ..... Signature redacted

Eveline Postelnicu
Department of Materials Science and Engineering
May 9th, 2017

Certified by ..... Signature redacted .....

Lionel C. Kimerling
Thomas Lord Professor of Materials Science and Engineering
Thesis Supervisor

Accepted by..... Signature redacted

Geoffrey Beach
Associate Professor Materials Science and Engineering
Chairman, Undergraduate Thesis Committee

Assessing materials quality for high efficiency electricity generation

by

Eveline Postelnicu

Submitted to the Department of Materials Science and Engineering
on May 10, 2017 in Partial Fulfillment of the
Requirements for the Degree of Bachelor of Science in
Materials Science and Engineering

ABSTRACT

Thermalization losses drastically reduce the efficiency of silicon solar cells. In an age where we need sustainable energy production more than ever, silicon is the best material to target due to its high stake in the sustainable energy market. An organic-inorganic solar cell hybrid of tetracene-covered silicon can reduce thermalization losses through the downconversion process of using a high energy photon to generate two lower energy electron-hole pairs. This occurs through the singlet-triplet fission process that excitons can undertake in tetracene. The effect of the interface quality between tetracene and silicon on successful triplet energy transfer is investigated. RFPCD (Radio Frequency Photoconductive Decay) is used to measure the bulk lifetime as well as the surface recombination lifetime of minority carriers in both n- and p-type Silicon of various doping concentrations. The surface recombination velocity was calculated from the measurement of surface recombination lifetime and analyzed after the silicon underwent RCA clean, RCA clean followed by an HF dip, tungsten nitride ALD, and tetracene evaporation using various combinations of these steps to form appropriate process flows. It was found that the highest surface quality was obtained by the lowest doped wafers. Additionally, similar doping levels were affected similarly by the various processing steps outlined above while the type of dopant did not seem to dictate the surface quality response. Triplet energy transfer was not fully confirmed from tetracene to silicon, but the surface quality turned out to be a very important indication for whether or not this energy transfer could occur.

Thesis Supervisor: Lionel C. Kimerling
Title: Thomas Lord Professor of Materials Science and Engineering

Acknowledgments

I would first like to thank Professor Kimerling for incredible thesis supervision and all of the time he has spent with me to fine-tune experiments and data analysis. I would also like to thank Professor Wada and Michel for their invaluable advice and support. A special thank you goes to all the students who helped me with all of the different lab experiments and responded to numerous emails titled URGENT – Neil Patel, Rushabh Shah, Danhao Ma, Peter Su, Qingyang Du, Derek Kita, and my collaborators Markus Einzinger, Cole Perkinson, and Tony Wu. Thank you to ASM inc. as well for the materials support. Lastly, many thanks to my family for more than proofreading and moral and emotional support. Thank you for inspiration and motivation, especially to my mother and Rachmaninoff's Concerto No. 2 in C Minor both of which without this thesis would not have occurred. Thank you!

Table of Contents

List of Figures and Tables

Introduction

Renewable energy sources are necessary now more than ever as our earth continues to suffer from the use of fossil fuels. Solar power provides a sustainable solution to the energy crisis. Silicon has dominated the solar power industry for years, and as a result is the most economically viable option to revolutionize our energy landscape. However, in order to propel this revolution, the thermalization losses silicon suffers must be addressed. My thesis will address improvements in silicon that reduce thermalization of carriers to the band edges after absorption by energies above the band gap of silicon (1.1 eV, 1127 nm).

The Schockley-Queisser limit on solar cell efficiency is about 32% due to blackbody radiation, recombination, and spectrum losses. [1] The materials employed in this thesis are Germanium (Ge) and Silicon (Si), with a primary focus on improving Si. Ge and Si both have indirect band gaps and thus require a phonon as well as a photon to result in solar-electric energy conversion. It is thus of the utmost importance to understand defects and how they can affect electron hole pair generation and recombination to attempt to exceed the Shockley-Queisser limit. Thermalization is another important area of concern. Only photons with energies larger than that of the band gap can generate electron-hole pairs. Thermalization occurs because electrons tend to occupy energy levels at the bottom of the conduction band and holes tend to occupy energy levels at the top of the valence band. The extra energy the carriers had from the photon is released as heat, or a phonon, in the lattice. [2] One way to reduce these losses is by using the "downconversion process" to generate two electron-hole pairs from photons with at least twice as much energy as the band gap of Si. The result is double the photocurrent output and an increase in the efficiency of Si in the high energy photon regime. Figure 1 depicts the part of the solar spectrum

from which silicon suffers thermalization losses. Ameliorating thermalization loss will increase the efficiency of a solar cell by targeting a large portion of these high energy photons.

One promising method of mitigating thermalization losses is through the use of multi-junction solar cells where an additional material grown on top of silicon can absorb these high energy photons. Another method which will be the focus of this thesis is photon fission resulting from exciton generation in organic materials. The material we will focus on in this study is tetracene, an organic molecule that absorbs high energy photons as excitons and which the Baldo group at MIT has hyptohesized will result in the transfer of two electron-hole pairs per absorbed photon due to singlet-triplet fission of excitons.

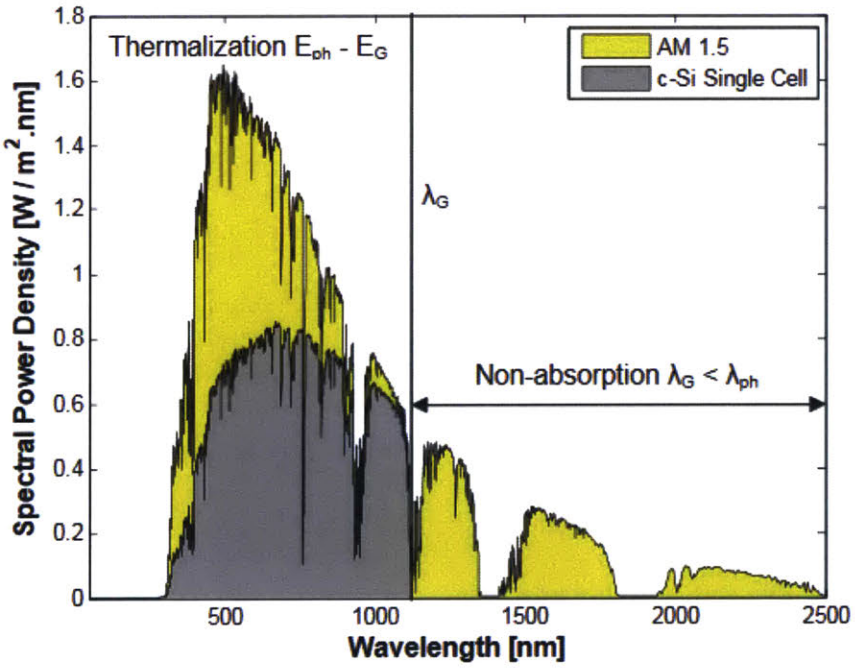

Figure 1. Spectral power density (intensity) vs wavelength with losses in efficiency indicated in yellow and thermalization losses indicated on the left side of the graph. [2]

The source of the two electron-hole pairs will be excitons generated in tetracene, an organic molecule placed on the surface of the silicon. Excitons are bound electron-hole pairs. In inorganic semiconductors, electrons and holes are delocalized and can easily separate to the conduction and

valence band. However, in organic semiconductors, electron-hole pairs are localized to either a single or a few molecules. An organic material absorbs a photon when an electron is excited from the highest occupied molecular orbital (HOMO) to the lowest unoccupied molecular orbital (LUMO), forming an exciton. Spin is very important in defining the energy states of this two-electron system. The lowest possible energy state is where both electrons occupy the HOMO. Because electrons are fermions, they have different spin so one is spin up $\left(s = +\frac{1}{2}\right)$ which is represented by ↑ and the other is spin down $\left(s = -\frac{1}{2}\right)$ which is represented by ↓. An excited state consists of an electron in the HOMO and one in the LUMO. The singlet state is the only excited state that displays an anti-symmetric spin configuration where $s_{total} = 0$.

$$\frac{1}{\sqrt{2}}(|\uparrow\downarrow\rangle - |\downarrow\uparrow\rangle) \qquad s = 0\ (single) \tag{0.1}$$

There also exists the possibility of three symmetric spin configurations for an excited state, where $s_{total} = 1$ due to the indistinguishability of electrons. These states are called triplet states [3].

$$|\uparrow\uparrow\rangle$$

$$\frac{1}{\sqrt{2}}(|\uparrow\downarrow\rangle + |\downarrow\uparrow\rangle) \qquad s = 1\ (triplet) \tag{0.2}$$

$$|\downarrow\downarrow\rangle$$

Singlet states cannot couple into triplet states nor can triplet states couple into singlet states upon interaction with light. Thus, a singlet ground state can only be excited into a singlet excited state and sees none of the triplet excited states as options. Because a singlet excited state can also only relax to a singlet ground state, triplet states cannot relax to the singlet ground state and have long lifetimes. Additionally, triplet states are lower in energy than singlet states and this difference in energy is dependent upon geometry and varies among molecules. [4]

In materials where the singlet state energy is about twice as large as the triplet state energy, two triplet states (T_1) can be generated from an excited singlet state (S_1) and a ground singlet state (S_0) through the process called singlet exciton fission (Figure 2).[5]

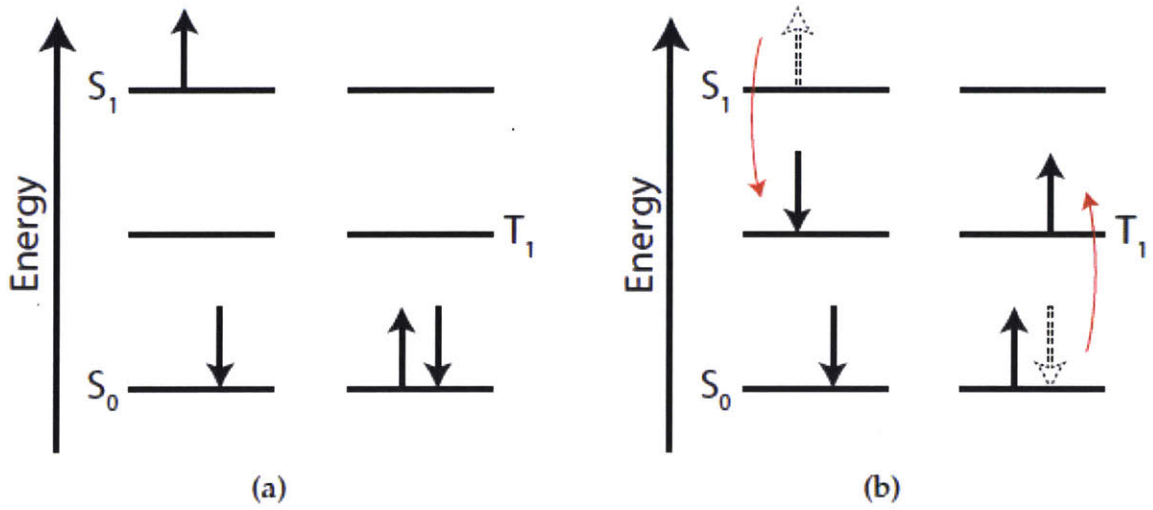

Figure 2. An excited singlet state, S_1 (a) can share its energy with the nearby ground singlet state S_0 to form two triplet states (b). [6]

Doubling the photocurrent from one photon is possible due to singlet fission. (Figure 3) Efficiencies above 100% for organic solar cells where pentacene undergoes singlet fission have already been demonstrated [7]. However, due to poorer efficiencies of organic solar cells compared to inorganic solar cells, the combination of an organic-inorganic solar cell is very exciting. Transfer of triplet states from an organic material, tetracene, to colloidal PbS quantum dots and from colloidal quantum dots into silicon have been shown to work [8,9], but no direct transfer from an organic molecule to silicon has been proven. Tetracene can absorb a photon of wavelength 350 nm and generate an exciton which will then undergo singlet fission. The two triplet states resulting from singlet fission can generate two electron-hole pairs silicon as if two photons of 700 nm light would have been absorbed by silicon. Tetracene's absorption of high energy photons and existence

of singlet states with twice the energy of triplet states make it the ideal candidate to test direct triplet transfer from an organic molecule to silicon.

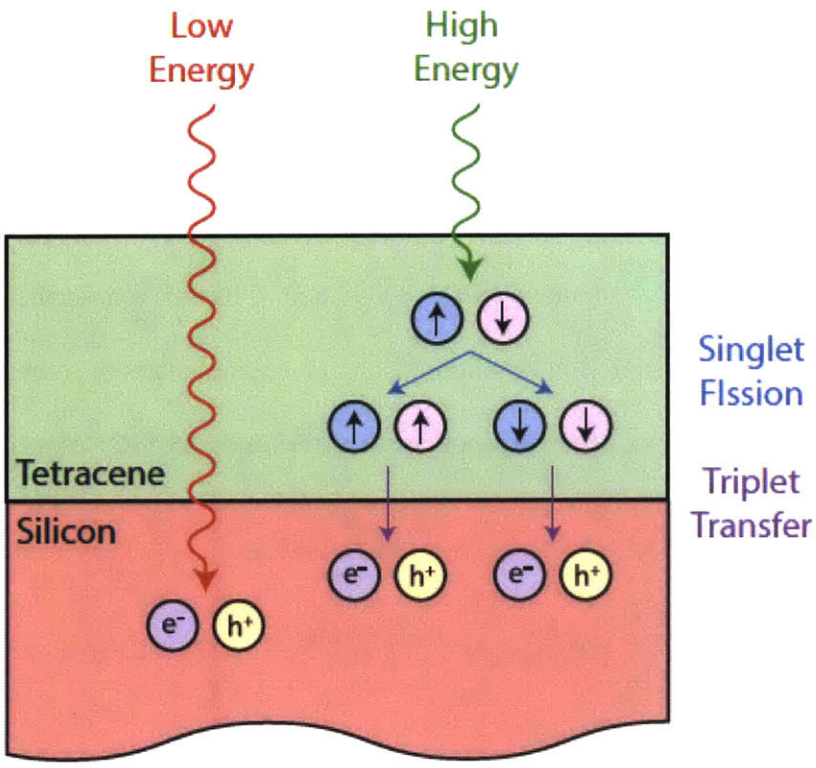

Figure 3. Schematic of low energy photons producing one electron hole pair in silicon and high energy photons undergoing singlet fission in tetracene, then producing two electron-hole pairs per one photon in silicon. [6]

The Baldo group's proposed tetracene-silicon junction has the potential to double the power output of a solar cell in the high-energy (low-wavelength) photon regime. Förster Resonance Energy Transfer (FRET) is the mechanism through which the exciton hops throughout tetracene. We expect the exciton to undergo tunneling within the first 10 nm of the silicon in its transfer from tetracene to silicon. However, the exciton's precise transfer mechanism from tetracene to silicon is unknown. As such, the surface quality of the interface between tetracene and silicon is of prime importance to the success of the energy transfer between these two materials. The focus of my work will be to investigate the parameters affecting interface quality and select

for the parameters that best ensure successful exciton transfer. This work is in collaboration with the Baldo group and builds significantly off of their previous collaboration with Neil Patel, '16 MIT PhD from the Kimerling group.

Chapter 1 describes the methodology behind Deep Level Transcience Spectroscopy (DLTS) and a model for the use of defect characterization to determine bulk lifetime. Chapter 2 details the use of Radio Frequency Photoconductive Decay (RFPCD) to determine surface lifetime and surface recombination velocity (SRV) of silicon. Chapter 3 describes the effect of surface treatment on the lifetime and SRV of silicon. Chapter 4 summarizes the connection between effects of tetracene deposition and processing on surface lifetime and SRV of silicon and triplet energy transfer.

Chapter 1: Using DLTS to determine bulk lifetimes and defect density

1.1 DLTS Background

Deep level transience spectroscopy (DLTS) can be used to characterize the bulk defects in a material by obtaining their activation energy, capture cross section, and thus the defect density. During DLTS, the sample is held under reverse bias and a voltage pulse is sent through the material at a certain rate. When the voltage increases, the junction is thrown out of reverse bias so the depletion width shrinks and carriers can flood the enlarged p and n regions of the material. When the pulse ends and the voltage goes back to the original voltage at reverse bias, the depletion width increases but some carriers remain trapped if there are defect states mid-gap. These carriers are excited to the conduction band through thermal emission. The capacitance across the junction is measured throughout the pulsing cycle. Because capacitance equals charge divided by voltage, the amount of charge and the rate at which the electrons are thermally emitted to the conduction band is directly proportional to the rate at which the capacitance transient decays.

1.2 Methodology

N-type Ge was irradiated with 6 MeV alpha particles at a dose of 5 $x10^8$ cm^{-2} to introduce defects. Conventional DLTS was first performed on the samples, followed by Laplace DLTS. Conventional DLTS pulses the voltage at a constant pulse width and measures capacitance while sweeping through a given temperature range. The transient decay rate is calculated over the same time interval at each temperature. At low temperatures, the rate of thermal emission will be low so the decay rate of the capacitance will be very low. As temperature increases, the emission rate will

increase until the temperature is so high that the transient decays very quickly and the time interval captured is past the point at which the electrons have been thermally excited to the conduction band. The emission rate of the defect can thus be determined by using the highest decay rate at a given temperature. Temperature is related to energy, therefore to the activation energy of the defect and thus its energy level can also be determined.

Next, Laplace DLTS is performed on the samples which keeps the temperature constant but varies the pulse widths at a given temperature. Varying the voltage pulse width means that the amount of time the junction is exposed to the voltage increase changes. By changing the amount of time the junction is thrown out of reverse bias, the amount of carriers that flood the junction and can thus remain trapped in the defect states, changes. The capacitance transient's decay rate is not only affected by the energy level of the defect state due to the Arrhenius relationship of energy and temperature, but also by the capture cross section of the defect state which means the concentration of defects present. A higher concentration of defects will mean more carriers are trapped in the defect which will change the amplitude of the transient. By comparing the saturation points of transients measured at different pulse widths, we can get an idea of the relative capture cross sections of the defects in the sample. Assuming the same recombination time for electrons and holes diffusing from mid-gap, the bulk lifetime can be estimated by

$$\tau_{bulk} = \frac{1}{\sigma \nu_{th} N_T} \tag{1.1}$$

where σ is the measured capture cross section, N_T is the defect concentration, and ν_{th} is the thermal velocity given by

$$\nu_{th} = \sqrt{\frac{3kT}{m_p^*}} \text{ . [10]} \tag{1.2}$$

1.3 Results from Germanium and proposed model for Silicon

One of the defects observed in Ge was E21, attributed to a mono-interstitial defect with capture cross section of $3.6 \times 10^{-20}\ cm^2$ and a defect concentration of $2.5 \times 10^{12}\ cm^{-3}$ [11]. The thermal velocity was calculated for the minority carriers involved in recombination (holes) and used to compute the bulk lifetime, about 0.2 s. The same model can be used to measure the bulk lifetime of silicon and its sensitivity to the kinds of defects introduced in silicon. The bulk lifetime measurements of silicon from DLTS can serve to substantiate those measured by RFPCD using HF passivation in Chapter 3.

Chapter 2: Using RFPCD to measure recombination time and SRV in Silicon

2.1 RFPCD background

An essential component of optimizing the interface between silicon and tetracene for excitonic transfer is being able to determine the quality of that interface by characterizing the surface states of the silicon. Radio frequency photoconductive decay (RFPCD) is a contactless measurement used to determine minority carrier lifetimes used to measure the nonequilibrium characteristics of the various silicon wafers used throughout this study. First proposed by Miller [12], the conductance of the wafer is inductively measured by using an radio frequency (RF) coil which acts as the primary of a transformer while the wafer undergoing the measurement is the transformer's short-circuited secondary. A general overview of RFPCD data collection is shown in Figure 4.

An LED light source above the wafer is used to optically generate excess carriers which increases the conductivity of the wafer. As the conductivity of the wafer increases, a current of corresponding magnitude to the conductivity of the wafer is induced in the RF coil, allowing us to measure the change in the wafer's conductivity as we pulse the light. A power source controls the current driving the LEDs which allows for modulation of the LED light intensity. The data acquisition is triggered by the light pulsing for an amount of time set by the user and gated at 500 microseconds to allow for carrier generation equilibration. The change in excess carrier concentration with time, which is proportional to the change in wafer conductivity, is given by:

$$\frac{d\Delta n}{dt} = G - U = G_{external} - \frac{\Delta n}{\tau} \tag{2.1}$$

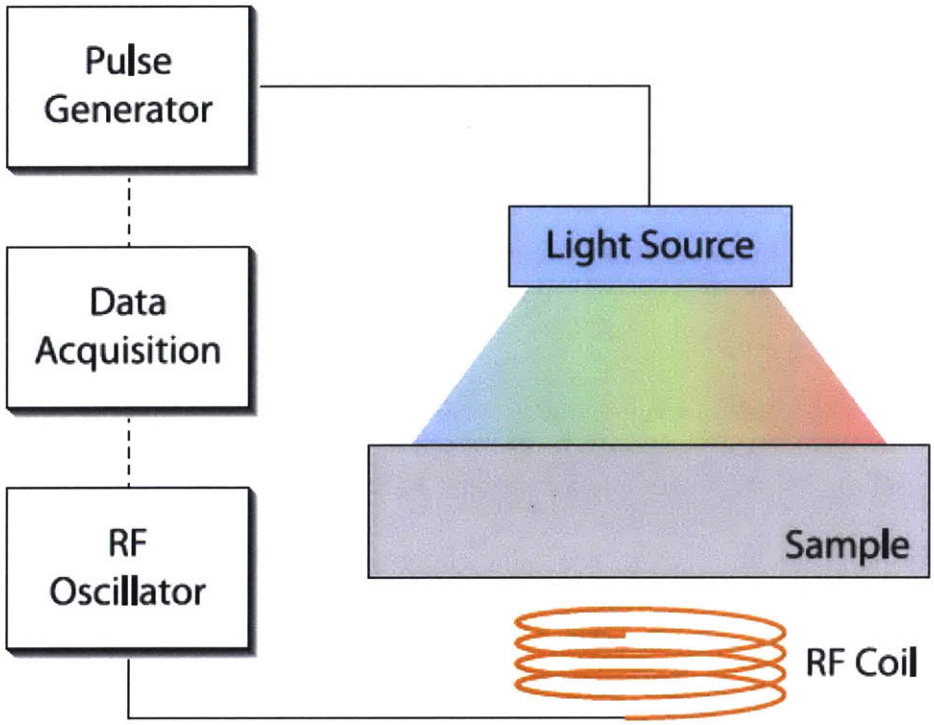

Figure 4. Schematic of RFPCD signal flow. The RF coil generates eddy currents that are affected by the sample's conductivity generated by the light source. The pulse generator pulses the light on and off while the data acquisition is triggered and the sample's conductivity is measured by the software. [6]

An LED light source above the wafer is used to optically generate excess carriers which increases the conductivity of the wafer. As the conductivity of the wafer increases, a current of corresponding magnitude to the conductivity of the wafer is induced in the RF coil, allowing us to measure the change in the wafer's conductivity as we pulse the light. A power source controls the current driving the LEDs which allows for modulation of the LED light intensity. The data acquisition is triggered by the light pulsing for an amount of time set by the user and gated at 500 microseconds to allow for carrier generation equilibration. The change in excess carrier concentration with time, which is proportional to the change in wafer conductivity, is given by:

$$\frac{d\Delta n}{dt} = G - U = G_{external} - \frac{\Delta n}{\tau} \tag{2.1}$$

where g is the generation rate due to the LED light source. If the illumination were kept constant during excitation ($G_{external} = g$) then

$$\Delta n = g\tau(1 - e^{-\frac{t}{\tau}}). \tag{2.2}$$

After illumination is removed (the light pulse ends and), $g = 0$ and

$$\Delta n = g\tau e^{-t/\tau}. \tag{2.3}$$

The τ in the above equations is the characteristic time decay constant of the carriers, or the minority carrier lifetime before recombination occurs. Figure 5 illustrates the RFPCD signal and its dependence on the generation rate, g, and τ, the effective carrier lifetime.

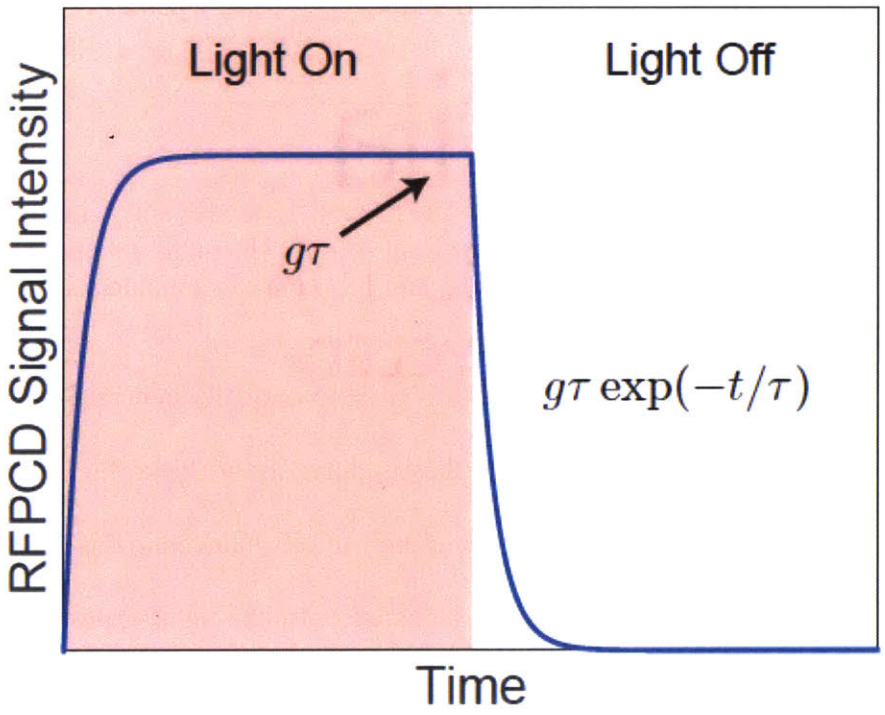

Figure 5. RFPCD signal. Conductivity increases when the light pulse is on and carriers are generated. Conductivity, and thus, generation, plateau at a value of $g\tau$. The light pulse turns off and the conductivity decays as carriers recombine. The time constant of the decay is characteristic of the minority carrier recombination lifetime in the sample. [6]

However, the effective lifetime measured contains contributions from both the bulk and surface recombination times.

$$\frac{1}{\tau_{eff}} = \frac{1}{\tau_{surface}} + \frac{1}{\tau_{bulk}} \tag{2.4}$$

For bulk lifetimes greater than 1 ms, the contribution of the bulk to the effective lifetime is negligible. Thus, minority carrier lifetime measured is the time it takes carriers to recombine at the surface. The Baldo group has estimated that the exciton will undergo tunneling from tetracene to silicon within the first 10 nm of the silicon surface. [6] Thus in this work we are primarily concerned with the requirements of the surface recombination lifetime and surface recombination velocity to ensure exciton transfer.

2.2 SRV requirements

RFPCD ideally measures the number of generated carriers. While one would expect the RFPCD signal to increase if exciton transfer is occurring between tetracene and silicon and stay the same if it isn't, the sensitivity of the system to noise mandates that we set a few requirements for sample parameters that determine successful transfer. Neil Patel, PhD '16 MIT, developed the model for SRV requirements based on internal quantum efficiency of the solar cell. The internal quantum efficiency (IQE), is defined as:

$$IQE = \frac{\#\ of\ collected\ carriers}{\#\ of\ absorbed\ photons} \tag{2.5}$$

and represents the generated carriers who have successfully diffused to the junction, or been collected before they've recombined and thus become useless and impossible to be collected. The IQE is generally highest for wavelengths where carriers are generated within a diffusion length of the junction. The larger the wavelength, the further away from the junction the carrier is which means it has to diffuse for a lot longer before being collected so there's a higher likelihood it will find a majority carrier with which to recombine. Thus, the IQE decreases for longer wavelengths. The IQE also decreases for shorter wavelengths because the shorter the wavelength, the shorter

the penetration depth of the light so the carriers are generated nearer the surface. The closer the carriers are to the surface, the more likely they are to undergo recombination due to defects at the surface and thus avoid collection which leads to the decrease in IQE. [13]

The bandedge of tetracene is about 530 nm. In order to reap the benefits of tetracene coated silicon, we would expect that carriers generated within 10 nm of the surface of the silicon have an IQE of at least half that of silicon at 530 nm. If 100% of the carriers generated by tetracene were collected, we would see double the IQE of the bulk for 530nm due to singlet fission. Unfortunately for all the of the species on planet Earth, it is much more likely that the transfer yield of excitons is less than 100%, which implies that in order to determine that excitons have definitely transferred and have undergone the singlet fission process, we need to see an IQE that is at least larger than what we would see normally for silicon at that wavelength, 530nm. This means that if we had anything larger than the 1:1 ratio of photon to electron-hole pairs, we would know that singlet fission occurred. Thus, a surface carrier (exciton transferred carrier) IQE that is at least greater than half the bulk IQE at 530nm would demonstrate that the ratio of photons to generated electron-hole pairs must be greater than 1:1 and so proves singlet fission occurred.

Figure 7 shows the internal quantum efficiency's dependence on SRV (surface recombination velocity) for different wavelengths of incident light and their corresponding absorption depths in Silicon. The greater the SRV, the lower the IQE, because the carriers diffuse much faster to the surface and thus have a higher likelihood of being lost to recombination instead of collected.

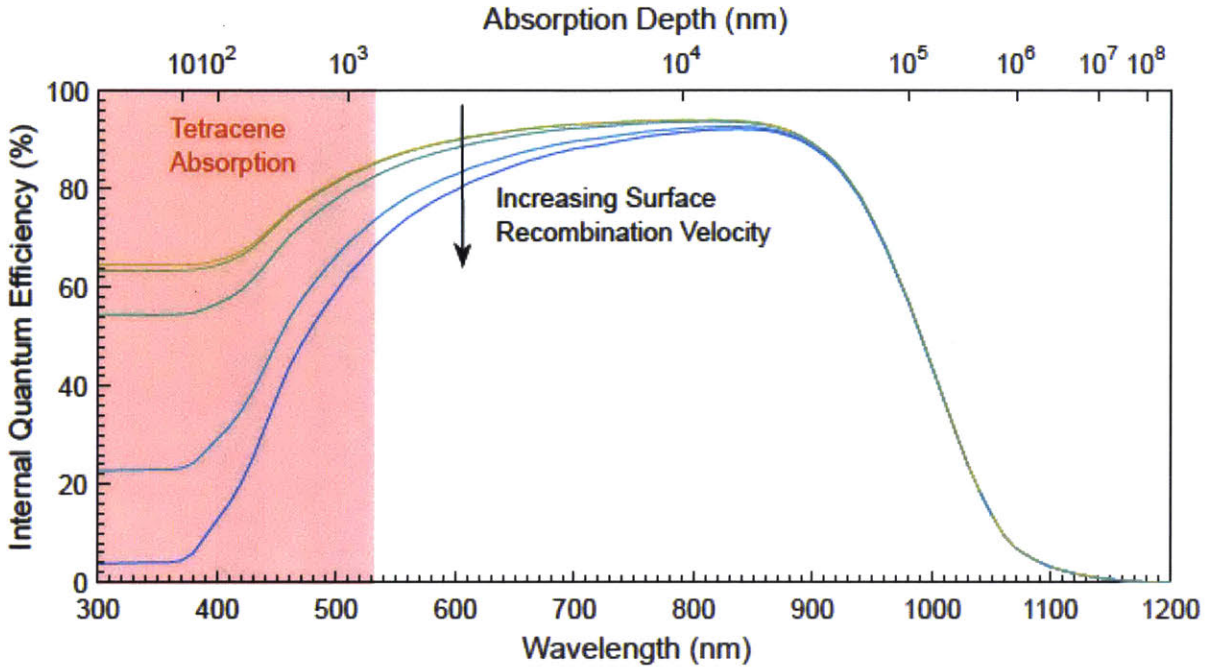

Figure 7. Internal quantum efficiency (IQE) vs wavelength for a typical Si solar cell with front surface recombination velocities varying from 10^2 cm/s to 10^6 cm/s. [6]

The simulation Dr. Neil Patel conducted using PC1D involved a standard solar cell (200 μm thick) with a n-type emitter doped to $4 \times 10^{19}\ cm^{-3}$ and a p-type base doped to $1 \times 10^{16}\ cm^{-3}$ and it assumed there is no surface recombination on the backside. Using Figure 7 and the IQE requirements discussed above, Dr. Patel modeled the IQE of surface carriers and the IQE from carriers generated at a wavelength of 530 nm as a function of SRV and emitter thickness (Figure 8) and determined that in order for the emitter thickness to remain less than 1 μm as is ideal, the SRV must stay below 10^4 cm for efficiency gains to still be seen. Figure 9 plots the IQE of surface carriers minus the IQE at 530 to demonstrate the chances in percentage that would occur in IQE. Taking into account triplet transfer efficiencies for two different emitter thicknesses in Figure 10, Dr. Patel concluded that the SRV should again be at most 10^4 cm/s to extract the most efficiency gains. Beyond that, the associated lower triplet transfer efficiencies actually reduce efficiency gains. [6]

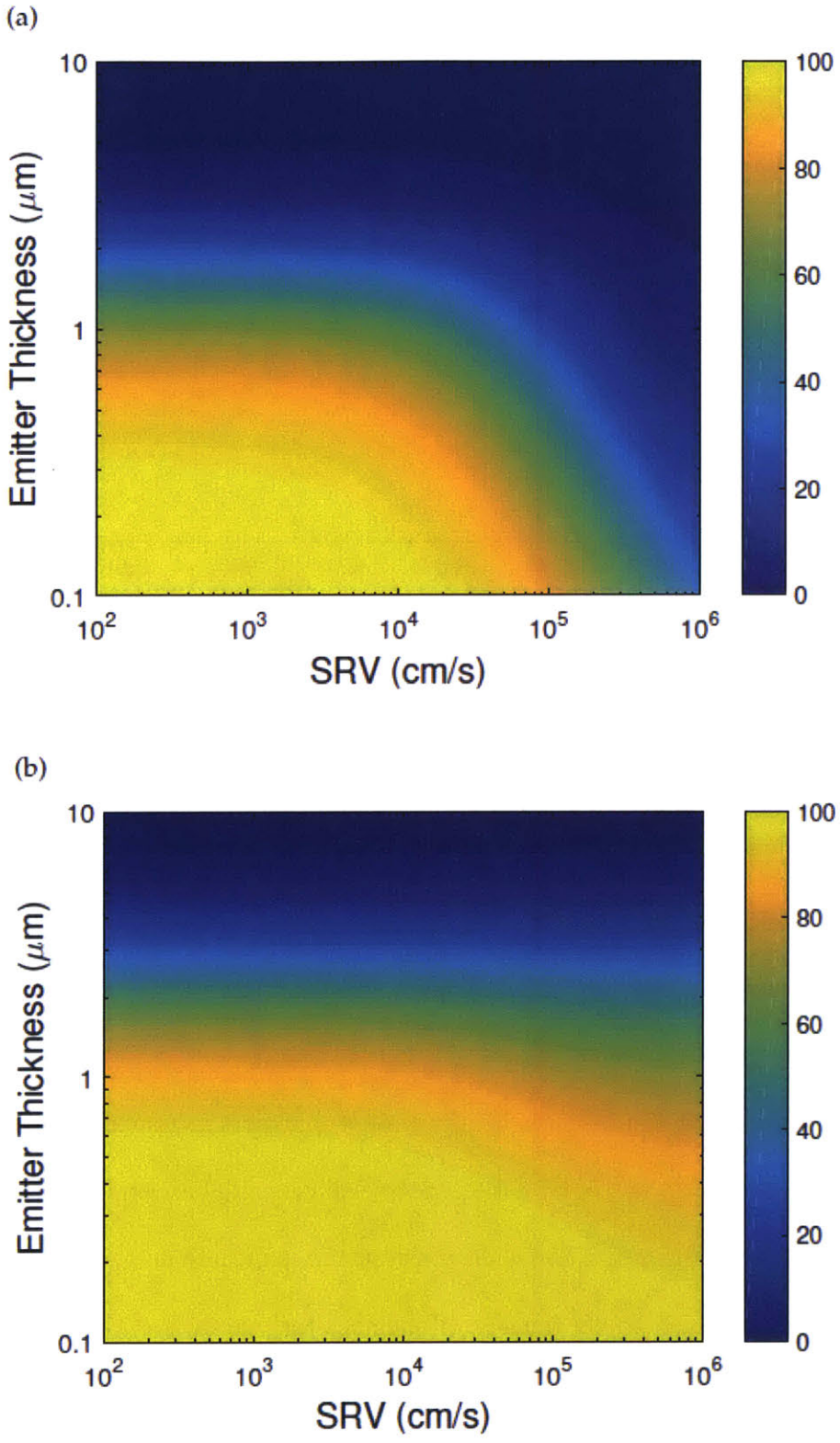

Figure 8. IQE for surface carriers (a) and 530nm (b) in a standard solar cell vs emitter thickness and front SRV [6]

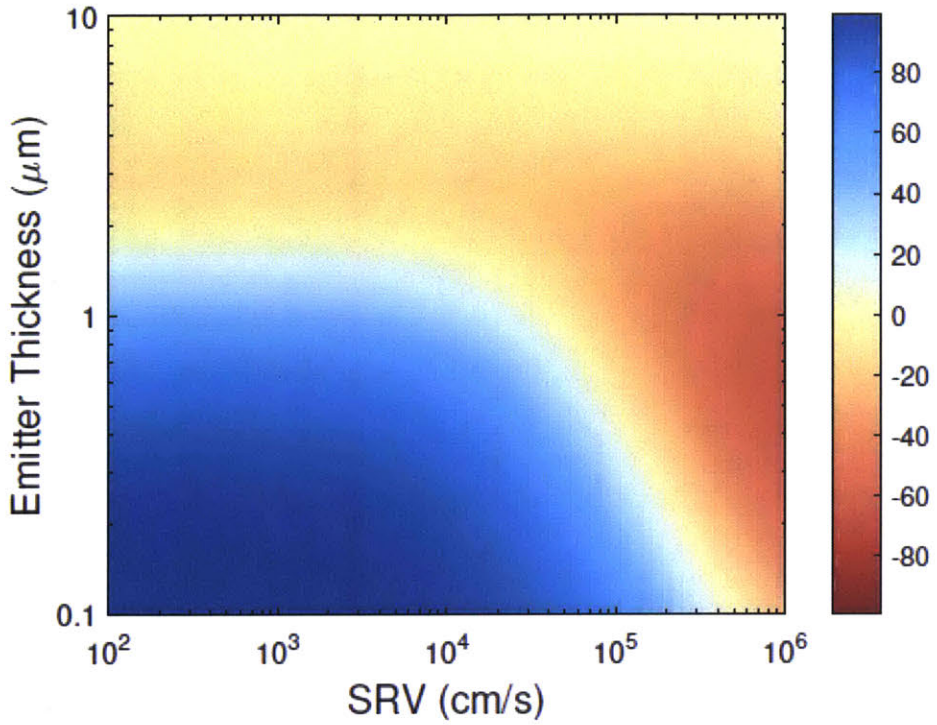

Figure 9. IQE of surface carriers generated by singlet fission minus IQE of 530nm in Si. [6]

The requirement for SRV to be greater than 10^4 cm/s in order for exciton transfer to be measured allows us to determine the necessary effective lifetime measurement from RFPCD that satisfies those restraints. The time it takes carriers to recombine at the surface measured with RFPCD which from now on will be called τ_{surf} and the SRV, S, are related through the transient equation:

$$\frac{1}{\tau_{surf}} = \beta^2 D \tag{2.6}$$

Where

$$\beta \tan\left(\frac{\beta d}{2}\right) = \frac{S}{D} \tag{2.7}$$

where D is the diffusion coefficient of the minority carriers in the wafer, and d is the wafer thicknesses. If the effective lifetime measured is larger than the time it takes carriers to diffuse to the surface, given by:

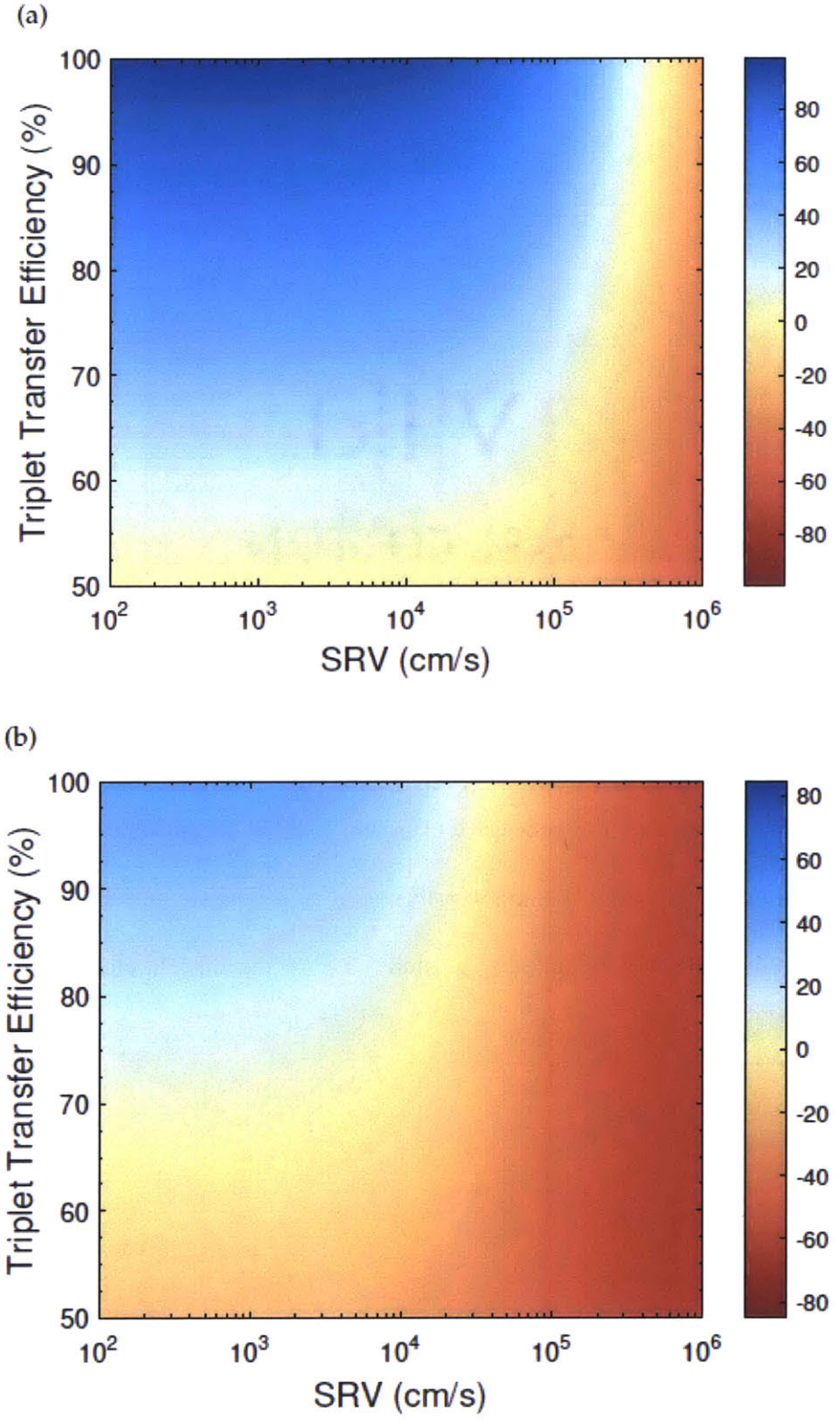

Figure 10. Effect of triplet transfer efficiency and SRV on the change in IQE from surface carriers to IQE minus IQE of 530 nm for a a) 1 μm emitter and a b) 100 nm thick emitter. [6]

$$\tau_{diff} = \frac{d^2}{\pi^2 D} \tag{2.8}$$

where d is the wafer thickness and D is the diffusion coefficient given by:

$$D = \frac{\mu k_B T}{q} \tag{2.9}$$

and μ is the mobility of the minority carrier of the wafer, k_B is Boltzmann's constant, T is temperature, and q is the charge of an electron, then we can say that surface recombination is not rate limited by diffusion. The surface recombination velocity, S, can then be approximated by:

$$S = \frac{d}{2\tau_{surf}} \tag{2.10}$$

2.3 RFPCD methodology

In order to determine the effect of processing on the surface quality of wafers employed in this work, RFPCD was conducted to obtain their effective lifetimes. For each of the wafers employed in this study, the time it would take carriers to diffuse to the surface was calculated to ensure that the measured lifetimes were greater and thus dominated by minority carrier surface recombination rather than diffusion to the surface (Table 1).

Sample ID	**Wafer thickness (μm)**	**Resistivity (Ohm-cm)**	**Doping density (cm^{-3})**	**Minority carrier mobility ($cm^2 V^{-1} s^{-1}$)**	**τ_{diff} (μs)**
HiRes n-type	675	>10000	4.4×10^{11}	1414	1.26
ASM n-type	775	35	1.25×10^{14}	1401	1.68
ASM p-type	775	500	2.65×10^{13}	469	5.02
Baldo p-type	675	10-20	1×10^{15}	461	3.87

Table 1. Wafers used in this work and their characteristic minority carrier diffusion time.

Because all diffusion times from Table 1 are greater than the measured effective lifetimes and the bulk lifetimes were determined to be less than 1 ms for all wafers involved in the experiment (see chapter 3), we know that the effective lifetime measured by RFPCD is indeed the lifetime of

carriers at the surface. The bulk lifetime is so large it has very little influence on the measured lifetime and the lifetime is clearly not diffusion-limited. The SRV is thus inversely proportional to the measured lifetime and so the measured lifetime can be used as a good indication of surface quality throughout the study.

Each sample was exposed to a 1 ms light pulse (Figure 5). The light pulse was longer than the sample lifetime so that carrier generation could saturate. The RFPCD amplitude would thus be indicative of the generation rate. Data was collected using LabView for long (9000 μs) and short (2000 μs) acquisition times which were then fit to a double and single exponential model, respectively, using Matlab. While the long pulse wasn't long enough to give an accurate indication of bulk lifetime, the long acquisition time substantiated the claim that the short lifetime measured was the lifetime of carriers at the surface by demonstrating goodness of the double exponential fit. The short acquisition time where the signal was cut off at 2000 μs was used to obtain more points along the fast decay for a more accurate measure of the lifetime of carriers at the surface. Figure 11 is an example of a typical decay fit using Matlab.

Single exponential: $A\exp(-B\cdot x)+C, \tau_{surf}=\frac{1}{B}$ (2.11)

Double exponential: $A\exp(-B\cdot x)+C\exp(-D\cdot x)+E, \tau_{surf}=\frac{1}{B}, \tau_{bulk}\sim\frac{1}{D}$ (2.12)

Not only was RFPCD used to determine the lifetime of carriers at the surface and thus the SRV, but the amplitude from RFPCD is proportional to the generation rate of carriers (section 2.1) and so can be used to determine whether or not energy transfer has occurred. Samples were first measured out of the box with no surface prep, then after an RCA clean, then after deposition of tungsten nitride (WN) used to improve tetracene adhesion, and finally after tetracene deposition. The RFPCD measurements prior to tetracene deposition were used to establish a baseline generation rate to compare with the generation rate after tetracene deposition.

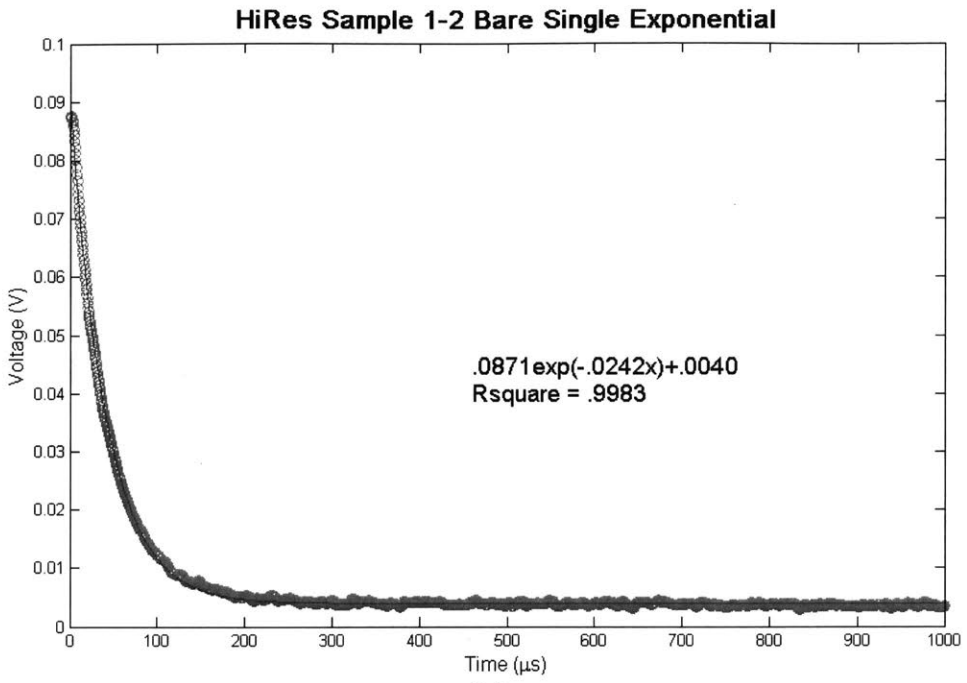

(a)

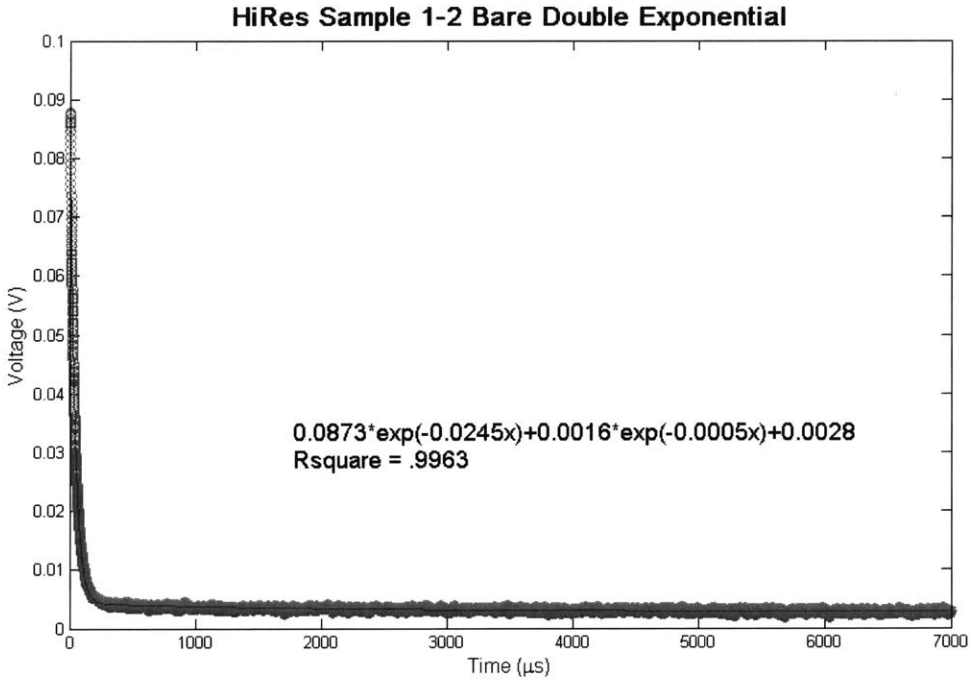

(b)

Figure 11. Example of a single (a) and double (b) exponential fit of the same sample using Matlab. RFPCD signal to decrease from tetracene's absorption of light which can be estimated from the

The samples were measured using 470 and 850 nm light. Silicon absorbs both these wavelengths of light, but tetracene only absorbs 470nm light. If no energy transfer has occurred,

we would expect the RFPCD signal to decrease from tetracene's absorption of light which can be estimated from the Beer-Lambert law:

$$1 - \frac{I(d)}{I_0} = 1 - \exp(-\alpha d) \tag{2.11}$$

where $1 - \frac{I(d)}{I_0}$ is the fraction of absorbed light, d is the thickness of tetracene (20 nm), and α is the absorption coefficient of tetracene. If the generation rate ratio of samples with tetracene to samples without tetracene is larger than the fraction of absorbed light, then we know that energy transfer from tetracene to silicon has occurred.

However, just having a difference in generation rate smaller than the difference due to absorbed light by tetracene does not indicate that triplet energy transfer has occurred, specifically. Energy transfer could have been singlet energy transfer only which would generate one electron-hole pair in silicon per tetracene singlet. In order to determine whether triplet energy transfer has occurred, the generation rate ratio of samples with tetracene to samples without tetracene must exceed 1 because triplets arise from singlet fission, leading to two electron hole pairs generated in silicon per triplet if triplet energy transfer is occurring. The sample was always placed in the same location relative to the coil and the light source was always the same distance away from the sample to control for as many variables affecting generation of carriers as possible. Additionally, the spot size of light was uniform along the size of the sample so that all parts of the sample were illuminated evenly. The samples were measured with 470 nm and 850 nm light as an additional control. Because tetracene has no absorption of the 850 nm light, we would expect to see no change in generate rate for samples with and without tetracene. 470 nm light has tetracene absorption so we would expect to see a generation rate decrease if the light is absorbed by tetracene and triplet energy transfer is not occurring or a generation rate increase if triplet energy transfer to silicon is

indeed occurring. Figure 12 demonstrates the predicted signal differences one would observe for the scenarios outlined above.

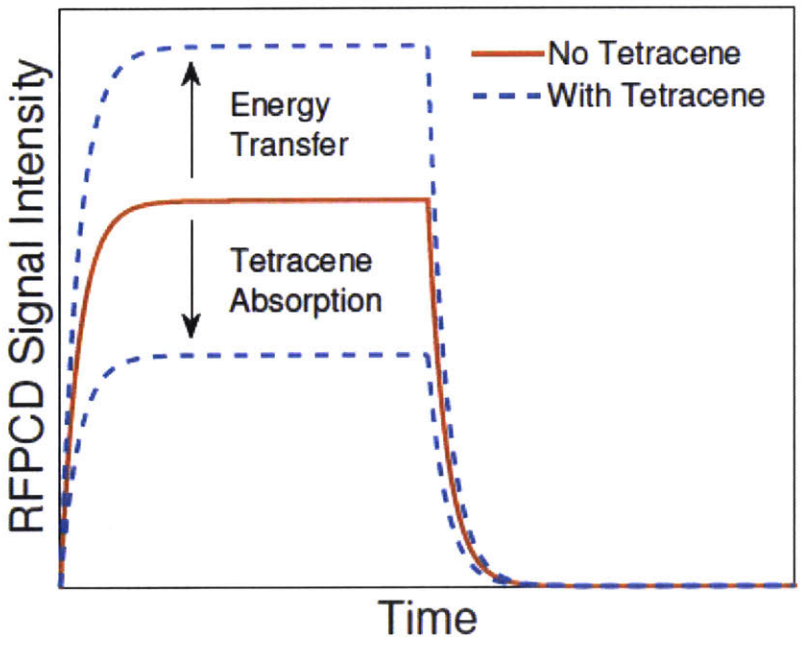

Figure 12. We would expect the amplitude of the RFPCD signal (the generation rate) to increase with triplet energy transfer and decrease if tetracene absorbs the light and triplet energy transfer is not occurring. [6]

2.3.1 RFPCD methodology validation

As this work serves as a continuation of Dr. Patel's preliminary work, the experimental set-up and Matlab script were verified by taking measurements of Dr. Patel's samples and comparing the results of my data collection with his. The samples used for methodology validation have an SiO_2 layer on the surface. If the surface is perfectly passivated by the oxide, we would assume the surface quality has not changed. Table 2 details the sample I measured, and the lifetimes obtained when I fit Dr. Patel's data of the sample with my own data of that sample. There are two lifetimes for each sample indicative of the double exponential model these samples obey. Despite one low percent difference of 73.9%, the remaining percent differences between the Patel

and Postelnicu measured lifetimes are all around 80% or higher. Because the thinner 50 nm oxide is subject to faster degradation, it is reasonable that the thinner 50 nm oxide exhibits a greater percent change in measured surface recombination lifetime. The high percentage correlation between the two independent measurements indicate the methodology I have described and followed throughout the thesis is sound.

Sample	λ (nm)	Patel lifetimes (μs)	Patel R^2	Postelnicu lifetimes (μs)	Postelnicu R^2	Percent change
50 nm SiO2 on FZ Si 6inch 60Amps	850	113.5	0.9999	143.0	0.9995	0.7390
		5095		5762		0.8692
	470	123.9	0.9999	143.0	0.9995	0.8458
		5537		5576		0.9930
100 nm SiO2 on FZ Si 6inch 60Amps	850	139.3	0.9996	168.1	0.9991	0.7933
		4763		4997		0.9508
	470	171.8	0.9997	168.5	0.9991	0.9808
		5436		4832		0.8888

Table 2. Comparison of measured lifetimes from Dr. Patel's data and Postelnicu's data collection.

2.4 RFPCD baseline results for wafers with no surface prep

In order to obtain tetracene-coated silicon wafers to study the potential for triplet energy transfer between tetracene and silicon, the wafers undergo several processing steps. The first step is an RCA clean (see chapter 3), followed by atomic layer deposition (ALD) of tungsten nitride (WN) that acts as a glue layer between silicon and tetracene, and finally, evaporation of tetracene. The wafers were first measured straight out of the box, with no surface prep, to construct the baseline of comparison for the rest of the processing steps. Table 3 summarizes the results for sample when measured with 850 and 470 nm light for short and long acquisition times then fit with the single and double exponential model described in section 2.3. Only the time it takes carriers to recombine at the surface, τ_{surf}, is reported. The bulk lifetimes are large enough

(Chapter 3) such that the indication of surface quality, SRV, is proportional to lifetime of carriers at the surface alone. Low R^2 values resulting from noisy measurements are omitted from this analysis due to the sensitivity of RFPCD. Thus, only fits with a 95% or greater R^2 value are considered. All of the measurements of bare wafers that have above a 95% R^2 value fall within the range of 40 to 115 μs, which corresponds to a range in SRV of 300 cm/s to 1000 cm/s.

Sample	Wavelength	Injection level (Amps)	τ_{surf} (us)	R^2	Exponential
HiRes Sample 1-2	850	70	40.87	0.9963	Single
	850	70	41.36	0.9983	Double
	470	66	46.68	0.9628	Single
	470	66	54.64	0.9601	Double
HiRes Sample 1-3	850	70	41.16	0.9978	Single
	850	70	39.76	0.9967	Double
	470	66	44.43	0.988	Single
	470	66	45.83	0.9814	Double
ASM n-type Sample 11-1	850	70	52.43	0.9932	Single
	850	70	53.83	0.9196	Double
	470	66	172.9	0.5452	Single
	470	66	80.55	0.3769	Double
ASM n-type Sample 12-2	850	70	48.75	0.9336	Single
	850	70	50.60	0.9853	Double
	470	66	139.6	0.2453	Single
ASM p-type Sample 16-2	850	70	46.69	0.9123	Single
	850	70	45.22	0.9796	Double
	470	66	51.63	0.1015	Single
ASM p-type Sample 16-3	850	70	45.75	0.9933	Single
	850	70	44.84	0.9624	Double
	470	66	121.2	0.3210	Single
	470	66	136.0	0.1569	Double
Baldo p-type	850	70	101.1	0.9985	Single
	850	70	99.95	0.9989	Double
	470	66	114.8	0.9985	Single
	470	66	114.6	0.9987	Double

Table 3. Lifetimes of carriers at the surface taken with 850 and 470 nm light and fit with single and double exponentials for short and long measurements, respectively, of the decay.

While the resulting SRV from wafers with no surface prep should result in efficiency gains from triplet energy transfer, a lower SRV would still drastically increase those gains - thus motivating the need for surface cleaning and passivation. The bare Si surface has Si atoms with one or two unused valence bonds, termed 'dangling bonds' which can act as traps for carriers and increase the rate of surface recombination. Natural oxide formed by oxygen as well and impurities like metals on the surface also contribute to surface states that increase the rate of surface recombination [10]. The R^2 value is always lower for measurements taken using 470 nm light as the signal is noisier for that wavelength. This may be because the penetration depth of 470 nm light is lower than 850 nm light and thus carriers are generated closer to the surface. The closer to the surface carriers are generated, the more they are subject to recombination. The faster recombination occurs, the lower the signal level of the sample due to the amplitude's dependence on τ. The faster recombination occurring closer to the surfaces means lower recombination times for 470 nm light than for 850nm light. Thus, the lower 470 nm signal is closer to the noise level of the system (~.005 V). The samples that experienced very low R^2 values had signals close to this noise level, but the bare surface lifetime resulting from the rest of the samples still falls within these large confidence intervals.

Every effort was made to use the same sample through the process flow described above. However, at times this was impossible as certain cleaning steps had to be conducted within the same environment as and be follow by immediate deposition. The effect of location among the wafer was surveyed for the ASM n-type and ASM p-type wafers. Figures 13 and 14 show the cleaving map for each 2 in. x 2 in. sample that was used in the study. There was no statistically significant difference of lifetime measurement based on location for either the ASM n-type or

ASM p-type wafers (Table 4), thus we can assume a low margin of error for lifetime comparisons of different samples throughout future processing steps.

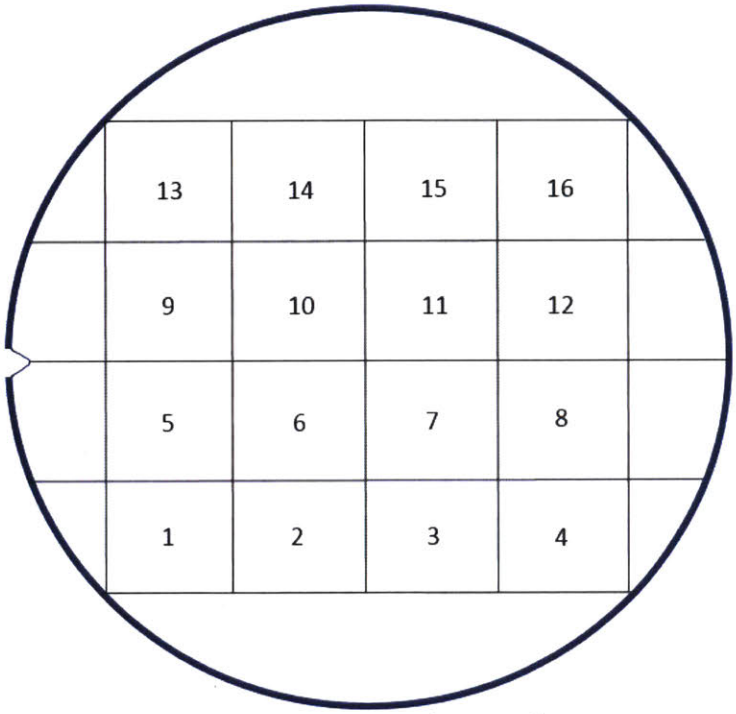

Figure 13. ASM n-type wafer sample map

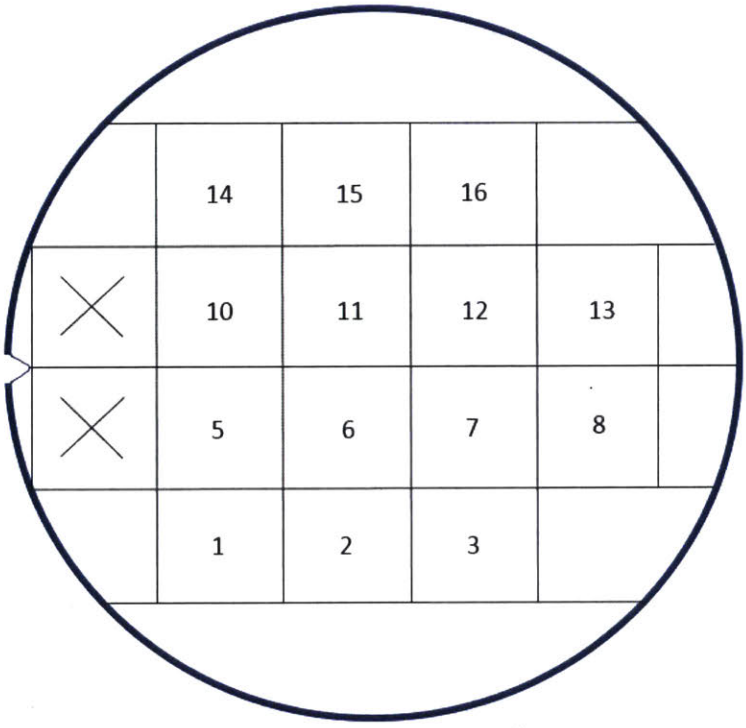

Figure 14. ASM p-type wafer sample map

Sample	Wavelength	Injection level (Amps)	n-type τ_{surf} (us)	n-type R^2	p-type τ_{surf} (us)	p-type R^2
1	850	150	54.00	0.9964	46.46	0.9984
	470	70	121.1	0.8951	51.58	0.9432
2	850	150	51.88	0.9965	45.94	0.9983
	470	70	106.51	0.889	85.06	0.5687
3	850	150	49.09	0.9979	45.61	0.9982
	470	70	62.91	0.7786	79.32	0.4494
4	850	150	51.76	0.9972		
	470	70	140.9	0.8976		
5	850	150	51.76	0.9972	45.74	0.9983
	470	70	100.7	0.8651	90.39	0.5185
6	850	150	51.16	0.9968	44.88	0.9983
	470	70	121.7	0.9012	66.42	0.5627
7	850	150	50.73	0.9967	46.54	0.9985
	470	70	130.7	0.878	55.42	0.5549
8	850	150	50.73	0.9967	45.41	0.9984
	470	70	103.1	0.9093	77.74	0.441
9	850	150	52.83	0.9969		
	470	70	103.7	0.8884		
10	850	150	52.27	0.9972	47.31	0.9988
	470	70	113.7	0.8827	61.19	0.568
11	850	150	51.81	0.997	42.50	0.9978
	470	70	103.3	0.8858	84.37	0.597
12	850	150	53.35	0.9963	46.62	0.9979
	470	70	103.5	0.8702	80.04	0.5486
13	850	150	52.83	0.9969	45.66	0.9982
	470	70	104.9	0.9096	87.02	0.4778
14	850	150	53.90	0.9961	44.84	0.9982
	470	70	105.8	0.8893	102.7	0.5462
15	850	150	52.70	0.9968	46.02	0.9981
	470	70	100.4	0.8583	105.5	0.5369
16	850	150	54.66	0.9963	45.50	0.9986
	470	70	110.7	0.8782	125.6	0.3961

Table 4. ASM n-type and p-type sample surface lifetimes, fit using a single exponential and measured with both 850 and 470 nm light.

We see again a general trend for lower R^2 with the 470nm light due to lower signal as the signal penetration depth is lower. However, while the p-type values for lifetime measured under 470 nm light are not statistically significantly different than the values measured under 850 nm

light, the n-type values measured under 470 nm light (~100 μs) are about twice as large as those measured under 850 nm light (~50 μs). One would expect the lifetime of carriers at the surface to increase as the carriers near the surface and interact with more recombination sites. Perhaps a natural oxide at the surface is causing this increase nearer the surface while the surface underneath is still dirty and unpassivated leading to the lower lifetime measurement of 50 μs.

Chapter 3: Effect of surface treatment on recombination time and surface recombination velocity in Silicon

3.1 Background on HF passivation

When a silicon wafer is placed in Hydrofluoric acid (HF), any oxide is removed and the surface is F-terminated. Fluorine weakens the silicon surface back bonds so that Hydrogen can come in and bond to the silicon, resulting in an H-terminated surface. Hydrogen thus saturates the dangling bonds responsible for recombination at the surface, allowing us to measure bulk lifetime using RFPCD. [10]

3.1 RCA clean

The RCA (Radio Corporation of America) clean is one of the most common cleaning procedures for silicon and a necessary step before HF passivation as described above as well as in the tetracene deposition by the Baldo group. The first step of the RCA clean is called Surface Clean 1 (SC1) and is a mixture DI water, ammonium hydroxide, and hydrogen peroxide in a 5:1:1 ratio. The second step is called Surface Clean 2 (SC2) which is a mixture of DI water, hydrogen chloride, and hydrogen peroxide in a 6:1:1 ratio. A dilute HF dip may or may not follow SC2. The solutions are heated to 80°C and the samples are left in SC1 for 10 minutes, rinsed with DI water, left in SC2 for 10 minutes, then removed and rinsed with DI water.

SC1 removes particles and organic compounds from the surface but leaves behind metallic contaminants due to the low solubility of metals in the SC1 solution which precipitate out as metal oxides. SC1 also roughens and etches the surface. SC2 removes the metal contaminants left behind by SC1. The HCl in SC2 decreases the reduction of metals and their

complexing to Cl^- and the presence of H^+ keeps metals in solution as ions and away from forming solids on the wafer surface. SC2 leaves a thin chemical oxide on the surface. The optional HF dip removes this oxide and leaves the surface hydrophobic. [10]

3.2 HF methodology

The samples were RCA cleaned to remove contaminants from the surface as described in Section 3.1 and then RFPCD was conducted while the samples were immersed in HF. The RFPCD equipment was moved to a hood and a Teflon beaker was placed on top of the coil. Teflon film covered the LEDs to protect them from the HF fumes. The sample was placed in the beaker and just enough HF was used to cover the sample completely. The sample's lifetime was measured using RFPCD and then the sample was rinsed with DI water and blown dry with nitrogen. Because the surface is very nearly perfectly passivated by HF, the SRV tends to 0 and the lifetime measured with RFPCD has the most contribution from the bulk lifetime rather than the surface lifetime.

3.3 Bulk lifetime results

HF passivation and subsequent bulk lifetime results from conducting RFPCD while samples were immersed in HF was used to confirm that the bulk lifetimes of all of the wafers employed in this work were larger than 1 ms such that the non-HF RFPCD was indicative of the lifetime of carriers at the surface. Figure 15 demonstrates the clear difference between the RFPCD signal of a non-HF passivated surface and complete HF passivation. The HF passivation measures the bulk lifetime, which is over 1 ms, and so never fully saturates for the 1 ms long light pulse employed during the measurement. The ramp-up to the plateau of generation rate is much longer as the recombination rate at the surface is almost 0. The decay is also much slower than the initial

decay measured without the samples immersed in HF. Table 5 summarizes the bulk lifetimes and resulting surface lifetime errors for all the wafer employed in this work except for the Baldo p-type. As 2-4 μs is within the noise of the equipment, the effective lifetime serves as a good indication of the surface lifetime.

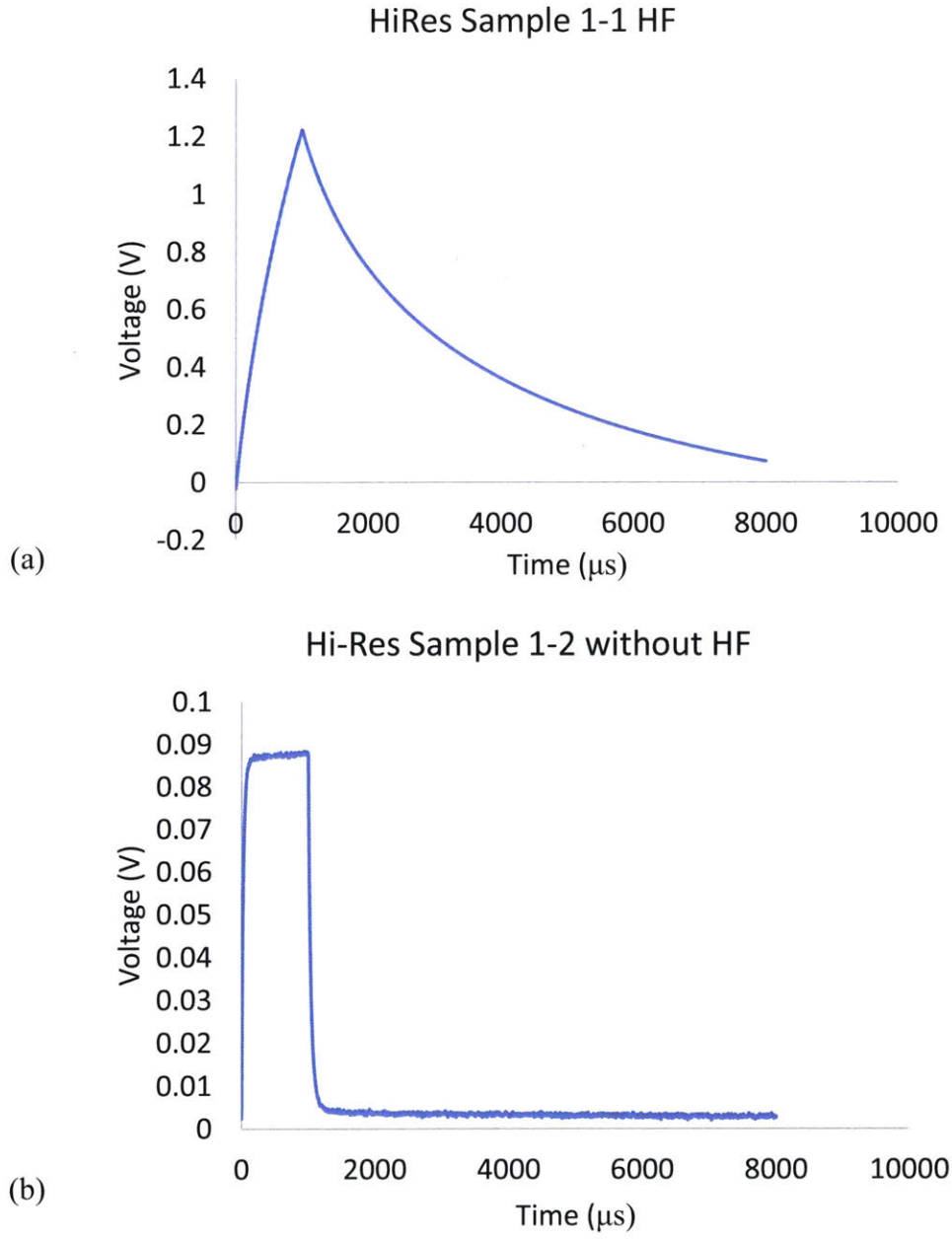

Figure 15. The plots demonstrate a sample from the same wafer, HiRes, measured while immersed in HF (a) and while measured normally, in air (b). The exponential decay is much slower and longer while measuring the bulk lifetime in (a) in comparison to the sharp initial decay of (b).

Sample	Wavelength	Injection level (Amps)	τ_{bulk}(us)	R^2	Error in surface lifetime (us)
HiRes Sample 1-1	850	150	2349	0.9972	2.7
ASM n-type Sample 12-1	850	150	1393	0.9989	4.4
ASM p-type Sample 16-1	850	150	2336	0.9979	2.6

Table 5. Measurement of bulk lifetimes and resulting overestimation in surface lifetime when taking the effective lifetime to be the surface lifetime.

3.4 Effect of RCA clean on surface lifetime

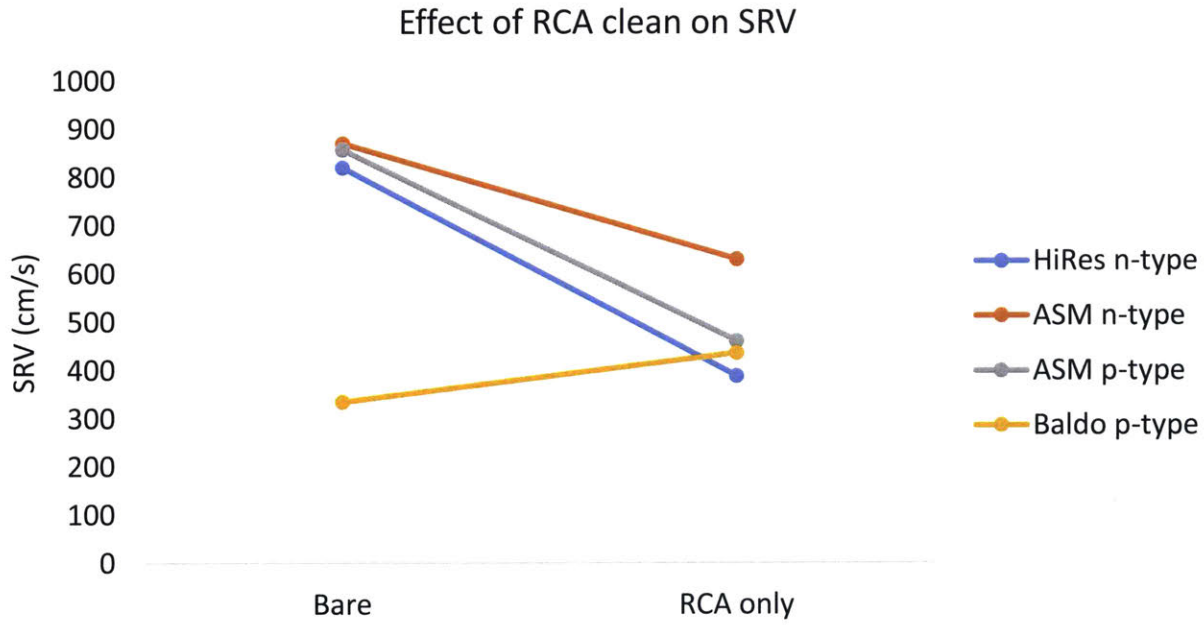

Figure 16. Effect of RCA clean on SRV using 850 nm measurements. RCA clean improved the surface quality of all wafers except for Baldo p-type, which aready had a low SRV thus a good surface.

The first step in silicon processing for tetracene deposition is an RCA clean to remove contaminants from the surface. For all of the wafers except the Baldo p-type, the RCA clean improved the surface quality (Figure 16). Only the lifetimes obtained using 850 nm light are

reported in Figure 16 as they had a consistently higher R^2 value than the 470 nm measurements and some of the 470 nm measurements were just noise and thus impossible to use.

The RCA clean was expected to improve the surface quality and thus lower the SRV as it rid the surface of impurities that could act as carrier traps and recombination centers. Perhaps the Baldo p-type's surface was already very good and only made worse by any contaminants the RCA deposited or by thin the chemical oxide deposited by the RCA clean. The Baldo p-type also had the highest doping, 10^{15}, of all the wafers, which may also contribute to the difference in the effect of RCA.

Chapter 4: Effect of Tetracene and Tungsten nitride on recombination time and surface recombination velocity in Silicon

4.1 Atomic layer deposition of Tungsten nitride

Tungsten nitride (WN) is used as a glue layer between silicon and tetracene and deposited using Atomic Layer Deposition (ALD) immediately after the silicon is RCA cleaned. The Baldo group graciously conducted the RCA clean and ALD for this work. ALD uses binary reaction sequences where two self-limiting surface reactions proceed in a sequential fashion allowing for precise thickness control of the deposited thin film. Not only can the thickness of thin films deposited through ALD be controlled at the atomic level, but the self-limiting reactions also result in very uniform and smooth layers. [14]

4.2. Evaporation of Tetracene

Following WN ALD, the tetracene is evaporated onto the surface using a thermal evaporator by the Baldo group. The thermal evaporation occurs in a vacuum chamber with a deposition pressure of less than 3×10^{-6} torr at a rate between 2 and 4 angstroms per second. The substrate holder was also rotated during the evaporation to result in a more uniform thickness. The thermal evaporator was also directly attached to a nitrogen glovebox where the tetracene-coated samples were encapsulated using UV curing epoxy and a quartz slip to prevent degradation of the tetracene film due to oxygen exposure. [15]

4.3 Methodology

The Baldo group conducted the deposition of both WN and tetracene with a few difference processing steps so that we could analyze the effect of each of the processing steps the samples underwent on the lifetime of carriers at the surface. The process flows were: 1) RCA with no HF dip then tetracene deposition, 2) RCA with no HF dip followed by WN ALD and then tetracene evaporation, and 3) RCA with an HF dip followed by WN ALD and then tetracene evaporation. Because the ALD required an RCA clean immediately before the ALD took place, we were unable to measure the same sample after RCA clean as well as after the WN deposition. Thus, one process flow includes only the effects of RCA which are considered to be fairly uniform among the wafer (see Section 2.4) and so can be attributed to the other process flows as well. The other process flows measure lifetime before any surface prep, and after RCA + HF +WN or RCA + WN when HF is not used as the last step in the clean. The measurements took about 30 minutes to conduct after each cleaning or deposition process, so some of the results may be affected by degradation of the RCA clean. The WN layer is stable for at least an hour, and the tetracene-coated samples were encapsulated and thus less susceptible to immediate degradation.

4.4 Effects of HF, Tungsten nitride, and Tetracene on surface lifetime

The RPFCD lifetime measurements were conducted and fit using a single and double exponential model using 850 and 470 nm light. The reported SRVS were calculated from the recombination time of carriers at the surface and plotted in Figures 17-20. The 850 nm single exponential fit was plotted for each processing step as the single exponential fit is more precise for surface recombination time. The 470 nm light resulted in very poor signal after a few of the processing steps and thus was not informative for lifetime trends.

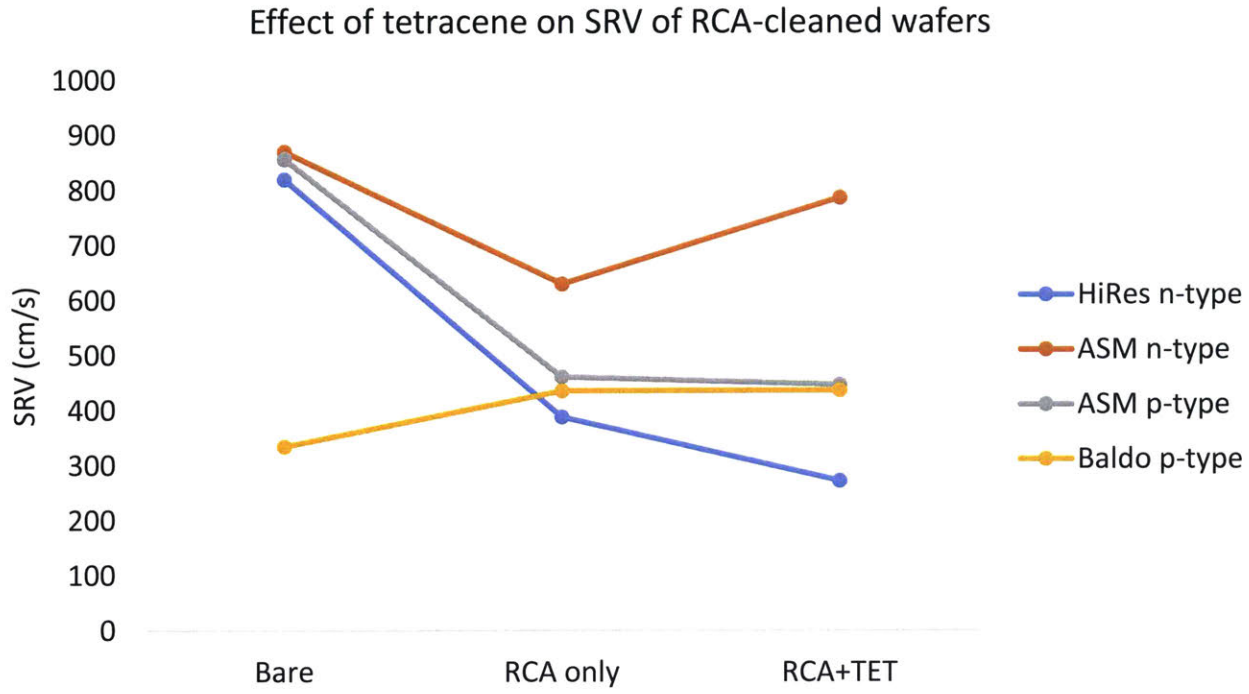

Figure 17. Effect of RCA clean and tetracene (Tet) deposition with no other HF dip or glue layer of WN on SRVs for 850 nm measurements.

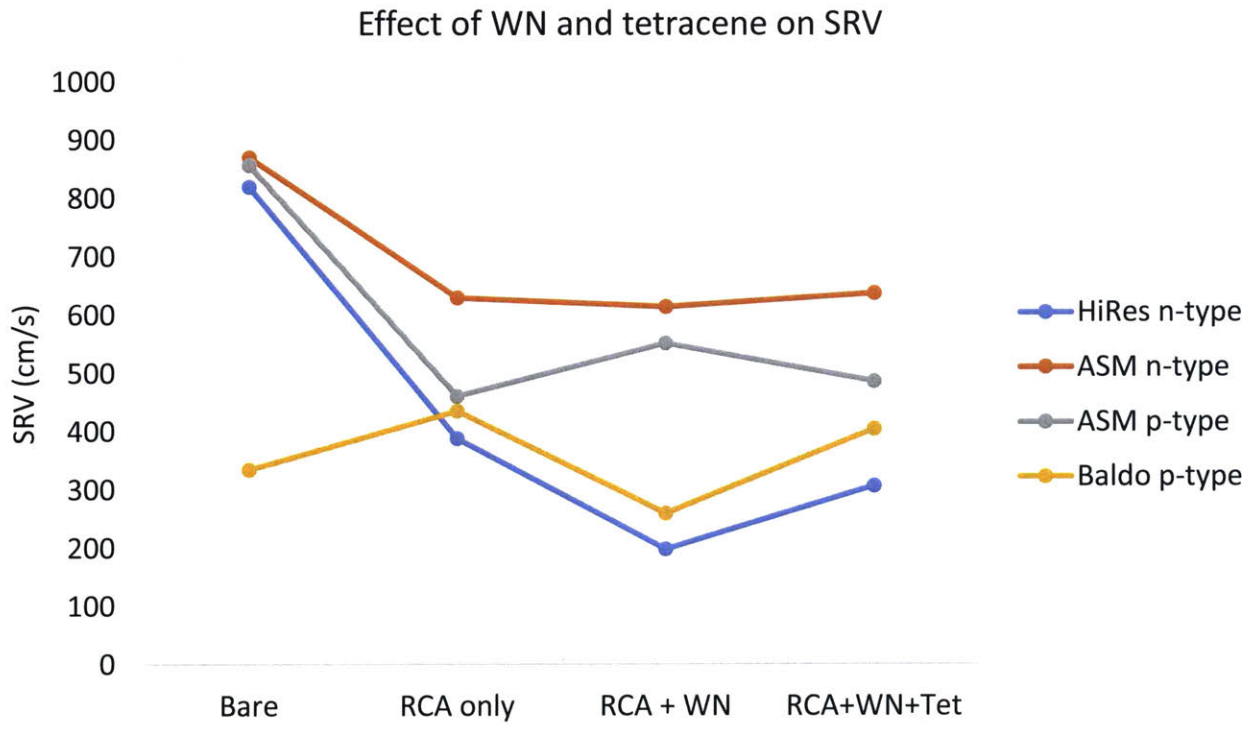

Figure 18. Effect of tungsten nitride and tetracene (Tet) deposition on surface quality of RCA-cleaned wafers with no HF dip for 850 nm measurements.

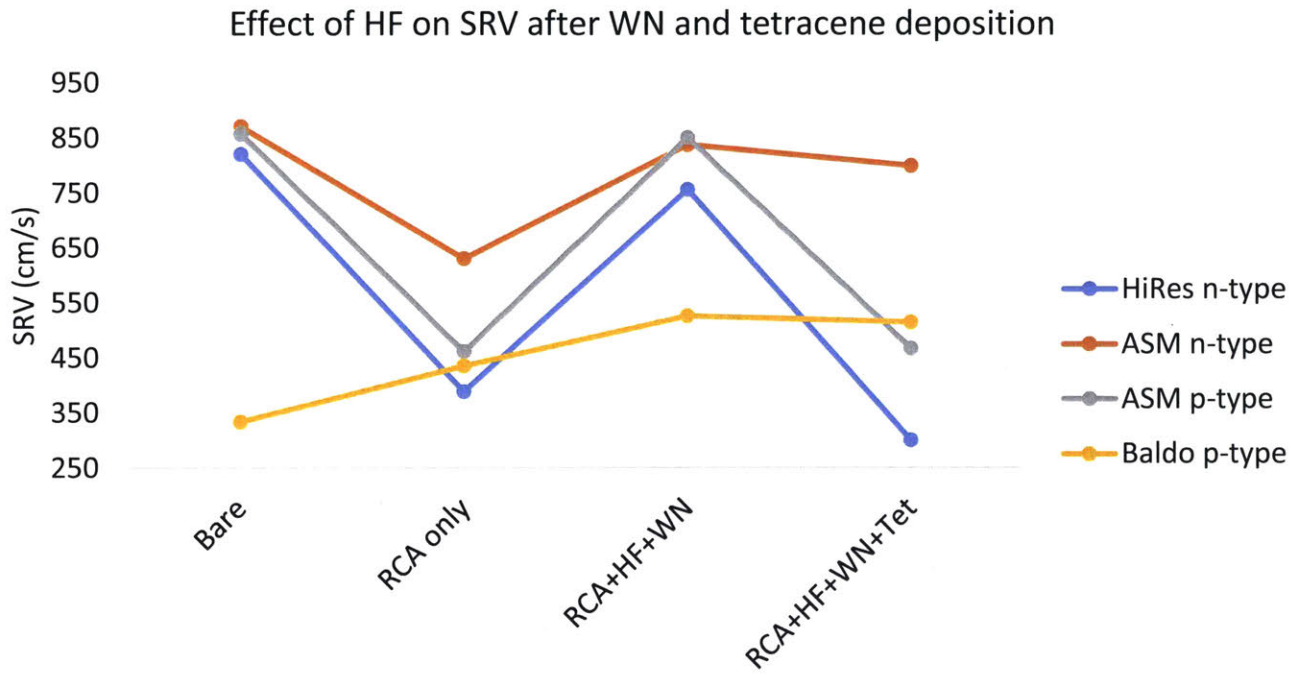

Figure 19. Effect of WN and tetracene (Tet) deposition on SRV of RCA-cleaned wafers with HF dip for 850 nm measurements.

.

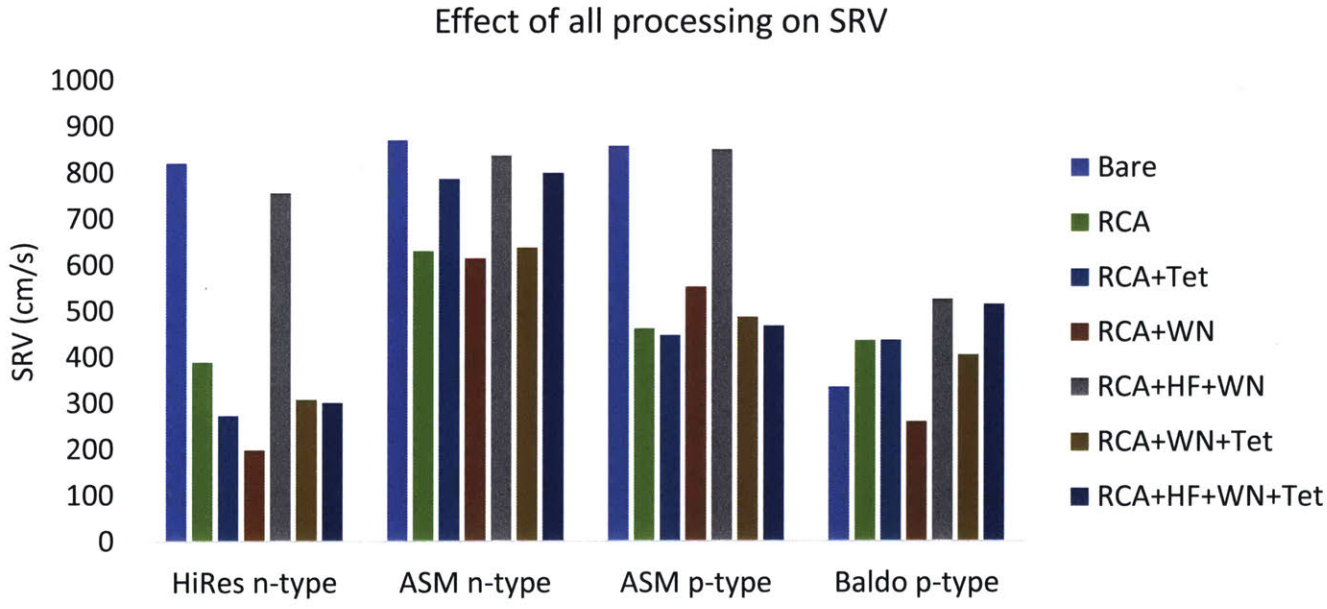

Figure 20. Comparison of all process flows with and without HF as well as with and without WN before tetracene deposition for 850 nm measurements.

Within the limited statistics of this study, tetracene deposition on the RCA-cleaned wafer surface with no WN adhesion layer resulted in high surface quality (low SRV) for the Hi-res n-

type sample and smaller increases in surface quality (lower SRV) for ASM p-type. The Baldo p-type and ASM n-type sample both exhibited a decrease in surface quality after tetracene deposition. This difference is consistent with the differences in doping for the sample set. Hi-res n-type has the lowest doping, 10^{11} cm^{-3} and ASM p-type is doped with 10^{13} cm^{-3}, while Baldo p-type has 10^{15} cm^{-3} doping and ASM n-type is doped with 10^{14} cm^{-3}. Band bending at the semiconductor surface can attract or repel charged carriers and influence their interaction with surface recombination sites and can determine SRV. The doping level and trapped surface charge control the extent and electric field of the band bending at the surface. In accumulation, minority carriers can be repelled from the surface. Similarly, the electrochemical potential gradient that drives carrier diffusion is less favorable with the larger barriers created by more band bending. The next round of experiments should explore doping and surface charge in a Design-for-Passivation experimental matrix. The key parameters are minority carrier diffusion to the surface or their electrostatic repulsion from the surface by trapped space charge. Since exciton energy transfer across the interface is governed by short range tunneling, the roles of recombination, surface charge and doping in the silicon final state's electron hole pair generation must be explored and put on a firm theoretical foundation.

For all samples except ASM p-type, ALD of WN improved the surface quality. The surface quality decreased very slightly for the ASM p-type and then increased again to the surface quality it achieved after the RCA clean with tetracene deposition. Tetracene deposition decreased surface lifetime after WN deposition for all wafers except ASM p-type but overall the RCA → WN → Tetracene process flow resulted in a higher surface quality for all samples except the Baldo p-type. The greatest positive increase in SRV occurred for the lowest doped wafers (HiRes n-type at 10^{11} cm^{-3} and ASM p-type at 10^{13} cm^{-3}). Perhaps the increase in SRV and thus surface quality after WN

deposition is due to passivation of the surface from the nitrogen in WN. Nitrogen has five valence electrons, one of which can bond to the silicon's dangling bonds on the surface and result in surface passivation. The fewer traps available for carriers at the surface in the form of dangling bonds, the better the surface quality.

The introduction of an HF dip after the RCA clean resulted in surprisingly low surface qualities for all samples followed by an increase in surface qualities for all samples following tetracene deposition (Figure 19). Among n- and p-type doping, the lower doped wafer's surface quality increased much more dramatically after tetracene deposition. Doping effects on band bending and the result for surface quality were previously discussed for Figure 17. The HF low lifetimes are surprising as we would expect HF to passivate the surface and result in a much higher quality surface, thus a longer surface lifetime. Perhaps the HF was contaminated with impurities that it then deposited onto the surface or it affected the uniformity or adhesion of the WN layer. Extra dangling bonds may have also resulted from saturating the silicon surface with passivation from the HF as well as the WN. The extra electrons from all of the passivating elements coating the silicon could act as traps for carriers in the same way dangling bonds would have without any passivation.

Though the surface qualities still increased after tetracene deposition, it can be seen from Figure 20 that the surface quality after tetracene deposition including the HF dip compared to the surface quality after tetracene with no HF dip was larger for the lower doped wafers out of our sample set (ASM p-type at 10^{13} cm^{-3} and HiRes at 10^{11} cm^{-3}). Meanwhile, the higher doped wafers (ASM n-type at 10^{14} cm^{-3} and Baldo p-type at 10^{15} cm^{-3}) exhibit the opposite – their surface qualities are better after tetracene deposition with no HF dip than with the HF dip. In fact, for all of the processing steps except the WN deposition after RCA, the surface qualities of the wafers

that are doped less than 10^{14} cm^{-3} (HiRes and ASM p-type) have the same directional (positive vs negative) response to the processing steps, at different magnitudes. Additionally, except for the very first RCA clean step, the wafers that are doped 10^{14} cm^{-3} or more (ASM n-type and Baldo p-type) show the same directional response at different magnitudes, for the remainder of the processing steps. It would seem that doping level controls the surface quality and its response to various surface cleaning methods and molecule depositions more so than the kind of dopant.

Another noteworthy point is that ASM n-type always exhibits the highest SRV, and thus the lowest surface quality. ASM n-type also had the lowest bulk lifetime of the measured bulk lifetimes, one ms below the rest of the samples. This difference in bulk lifetime could suggest that bulk lifetime plays a more significant role than was previously considered in surface quality. While HiRes n-type and ASM p-type exhibit a general trend towards better surface quality and Baldo p-type exhibits a trend towards worse surface quality in Figure 20, ASM n-type doesn't seem to exhibit any relevant trends. This could be due to the bulk lifetime's effect on surface quality or due to the fact that the bulk lifetime was lower meaning there is a greater error associated with taking the effective lifetime from RFPCD as the time it takes carriers to recombine at the surface. Perhaps the error associated with the lower bulk lifetime as well as the bulk lifetime's effect on surface quality both contributed to the murkiness of the processing steps' effects' analysis for ASM n-type.

4.5 Triplet energy transfer to Silicon

In addition to analyzing the effect on the surface quality by measuring the surface lifetime, the amplitude of the RFPCD signal along with the time it takes carriers to recombine at the surface was used to determine the generation rate and whether or not triplet energy transfer was observed.

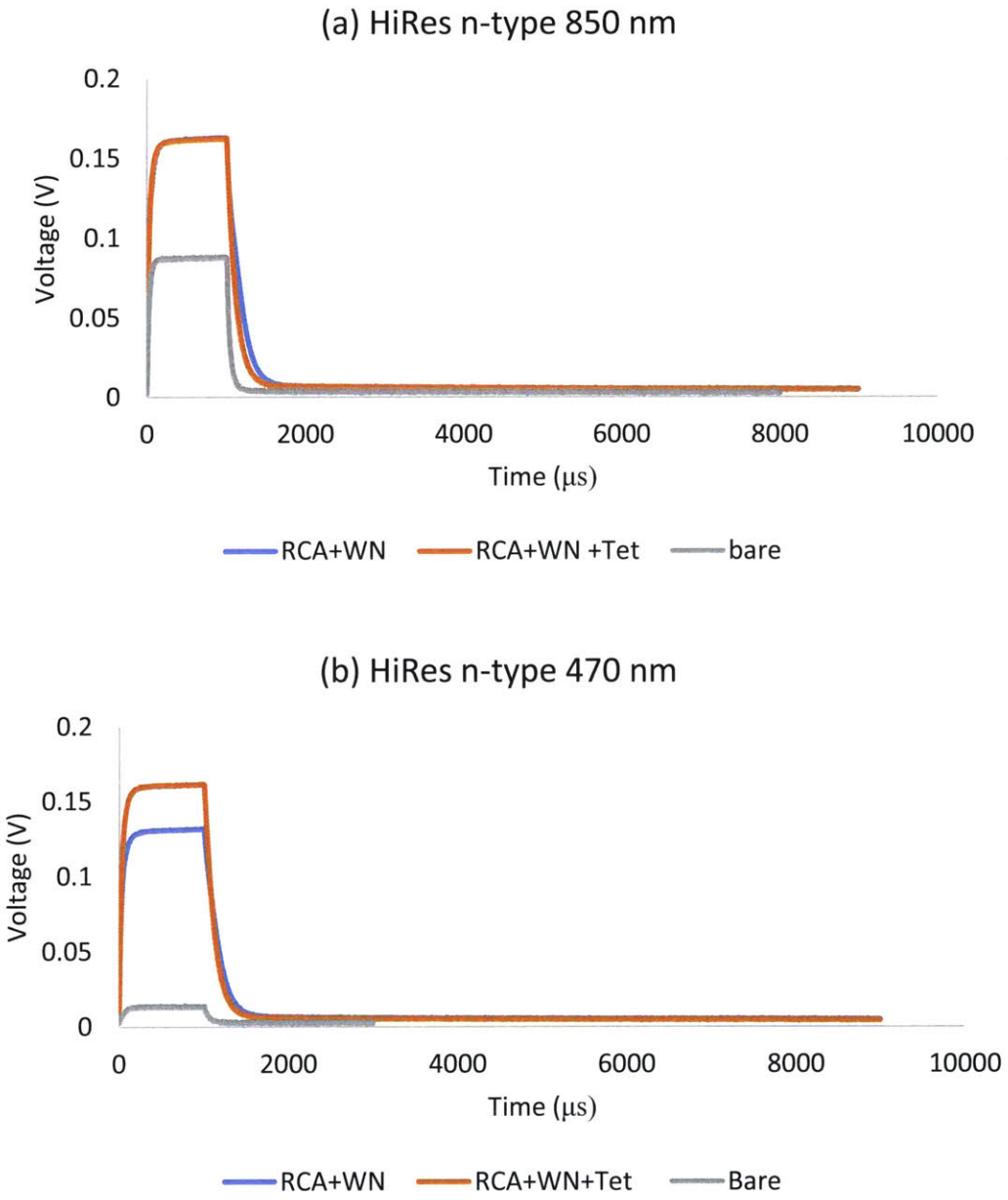

Figure 21. Evidence of triplet energy transfer from tetracene to silicon as excitation with 850 nm light results in a slightly lower amplitude than the processing step prior to tetracene deposition (RCA and WN ALD) (a) and excitation with 470 nm results in a much larger amplitude for the sample with tetracene that the prior processing step (RCA and WN ALD).

The only sample that behaved as we would expect if triplet energy transfer was occurring was the HiRes n-type (see Figure 21). The amplitude of the RFPCD plateau after tetracene deposition was not higher for 850 nm and was higher for 470 nm. We would expect this result if

tetracene was not generating extra carriers for 850 nm light and if triplet energy transfer was occurring due to extra carriers generated by the 470 nm light. We would in fact expect the RFPCD plateau to be lower than the initial signal for 850 nm light due to absorption of the light in tetracene.

Sample	Wavelength	Tet SRV (cm/s)	With tet g/without tet g
RCA only + Tetracene			
Baldo p-type	850	436.0	1.911
	470	411.8	1.136
ASM n-type	850	786.0	1.415
	470	720.1	0.484
ASM p-type	850	446.7	2.635
	470	443.4	1.424
HiRes n-type	850	271.8	1.441
	470	239.0	1.545
RCA + WN + Tetracene			
Baldo p-type	850	404.1	0.454
	470	367.0	0.437
ASM n-type	850	650.1	0.860
	470	567.2	0.739
ASM p-type	850	485.9	0.514
	470	466.5	0.506
HiRes n-type	850	306.5	1.547
	470	294.1	1.680
RCA + HF + WN + Tetracene			
Baldo p-type	850	514.1	1.256
	470		
ASM n-type	850	798.4	1.190
	470		
ASM p-type	850	466.3	0.820
	470		
HiRes n-type	850	300.2	0.662
	470		

Table 6. Surface recombination velocity (SRV) for each sample after tetracene deposition, the final step in the process and with tetracene to without tetracene generation rate ratio for each sample. Values that are missing are due to extremely large noise and poor signal such that the information is completely lost among the noise.

However, as the peak of the RFPCD signal is proportional to generation rate multiplied by the surface lifetime, the surface lifetime and thus the quality of the surface also affects the amplitude of the signal and not only the generation rate. In order to confirm that triplet energy transfer was occurring, the SRV and ratio of generation rates of the final tetracene deposition to the processing step right before the tetracene deposition was computed for every sample and summarized in Table 6.

The only samples that exhibit a larger generation rate ratio of with tetracene to without tetracene under 470 nm excitation than 850 nm are the HiRes n-type samples that underwent an RCA clean and a tetracene deposition, and an RCA clean, ALD of WN, and tetracene deposition (see highlighted values in Table 6). These samples also exhibit the lowest SRVs and thus the best surface quality after tetracene deposition of the entire sample space. Recall that our requirements to prove that triplet energy transfer had occurred were that: 1) the generation rate ratio of with to without tetracene is lower for 850 nm light and higher for 470 nm light; and 2) the generation rate ratio of with to without tetracene is above 1 for 470 nm light is the HiRes n-type that resulted from the RCA + WN + Tetracene process flow. While both conditions seem to be satisfied for triplet energy transfer to have occurred according to the 470 nm light measurement, the generation rate of 850 nm should not exceed 1 as it does for the HiRes n-type samples. The generation rate should in fact be lower than 1 as tetracene absorbs some of the incident light leading to a lower generation rate. The Baldo group predicts about a 1% in efficiency if triplet energy transfer occurs at its best triplet yield. The error in lifetime measurements is on the same scale as we would see with a 1% change in generation rate. The sensitivity in measurement required to thoroughly prove triplet energy transfer occurred may not be possible given these samples' SRVs and RFPCD ability. While triplet energy transfer was not completely validated

from the HiRes sample analysis, the SRV seems very important in obtaining a higher generation rate for 470 nm light than 850 nm light.

Conclusions and future work

This work investigated the materials quality parameters necessary to ensure triplet energy transfer from tetracene to silicon. The possibility of singlet fission in generating twice the number of electron-hole pairs in silicon when tetracene is excited by high energy photons was studied through the proposed use of DLTS to investigate bulk lifetime and the use of RFPCD to asses bulk lifetime and surface quality. It was determined that surface quality is of the utmost importance to successful triplet energy transfer as we expect tunneling to be an integral aspect of the energy transfer to silicon. Thus, the effects of the necessary processing to produce a tetracene-coated solar cell were investigated using RFPCD to assess SRV after each processing steps. It was determined that the deposition of WN was a high point for surface quality among all of the samples potentially due to the surface passivating effects of nitrogen on silicon. However, the introduction of HF after the RCA clean produced truly dismal surface qualities in all samples investigated in this work potentially due to competing passivation with nitrogen resulting in unbound electrons forming recombination sites at the surface. Doping concentration rather than dopant type seemed to dictate the SRV response to these various processing steps.

The lowest doped wafer, HiRes, exhibited the best surface quality at the end of the processing flow and also was the only sample that satisfied the first condition out of the two conditions for triplet energy transfer. These conditions were that the generation rate was higher for 470 nm light than 850 nm light and the generation rate was greater than 1 for 470 nm light and less than 1 for 850 nm light. The generation rate under 850 nm light excitation was greater than 1 for the HiRes sample potentially due to the error associated with the RFPCD measurement and the requirement for greater sensitivity to detect triplet energy transfer.

Future work would include trying to amplify the sensitivity of the measurement by introducing a lock-in amplifier to reduce noise. Additionally, the sample should always be placed in the exact same location and ensured it is the same height from the LEDs to obtain more accurate reference measurements. The intensity of the LED light should be calibrated using a photodetector to ensure even spot size over the entire sample. Fabrication of larger samples should also be considered so as edge effects involved in eddy current generation from the RF coil can be minimized. Additionally, the effect of bulk lifetime and overall material quality should be further investigated by obtaining more highly doped wafers to see if they follow the same non-trend-like behavior of the ASM n-type sample. Finally, further passivating layers such as SiO_2 and HfO_2 that are very thin to allow excitonic tunneling should be introduced as another surface processing step to determine surface lifetime. By increasing the time it takes carriers to recombine at the surface and thus decreasing the SRV, the error in lifetime measurements also decreases so the sensitivity issues may be mitigated.

While triplet energy transfer was not completely confirmed by this work, it is clear that the surface quality of the interface is drastically impacted by the processing. Interface quality and effective processing thus become very important features to keep in mind in order to achieve high efficiency electricity generation in organic-inorganic compound solar cells through the revolutionary process of photon fission.

Bibliography

1. Shockley, William, and Hans J. Queisser. "Detailed Balance Limit of Efficiency of p-n Junction Solar Cells." *Journal of Applied Physics* 32.3 (1961): 510-19. Web.

2. "Chapter 5: Solar cell conversion-efficiency limits", retrieved from http://aerostudents.com/files/solarCells/CH5SolarCellConversionEfficiencyLimits.pdf

3. D. J. Griffiths, *Introduction to Quantum Mechanics*, 2nd edition. Upper Saddle River, NJ: Pearson Prentice Hall, Apr. 10, 2004, 480 pp.

4. H. Uoyama, K. Goushi, K. Shizu, H. Nomura, and C. Adachi, "Highly efficient organic light-emitting diodes from delayed fluorescence", *Nature*, vol. 492, no. 7428, pp. 234–238, Dec. 13, 2012. doi: 10.1038/nature11687.

5. M. B. Smith and J. Michl, "Singlet Fission", *Chemical Reviews*, vol. 110, no. 11, pp. 6891–6936, Nov. 10, 2010. doi: 10.1021/cr1002613.

6. Patel, Neil, *Understanding Defects in Germanium and Silicon for Optoelectronic Energy Conversion,* Thesis (Ph.D.) – Massachusetts Institute of Technology, Dept. of Materials Science and Engineering, 2016.

7. Pazos-Outón, Luis M., Ju Min Lee, Moritz H. Futscher, Anton Kirch, Maxim Tabachnyk, Richard H. Friend, and Bruno Ehrler. "A Silicon–Singlet Fission Tandem Solar Cell Exceeding 100% External Quantum Efficiency with High Spectral Stability." *ACS Energy Letters* 2.2 (2017): 476-80. Web.

8. N. J. Thompson, M. W. B. Wilson, D. N. Congreve, P. R. Brown, J. M. Scherer, T. S. Bischof, M. Wu, N. Geva, M. Welborn, T. V. Voorhis, V. Bulović, M. G. Bawendi, and M. A. Baldo, "Energy harvesting of non-emissive triplet excitons in tetracene by emissive PbS nanocrystals", *Nature Materials*, vol. 13, no. 11, pp. 1039–1043, Nov. 2014. doi: 10.1038/nmat4097.

9. A. Yeltik, B. Guzelturk, P. L. Hernandez-Martinez, A. O. Govorov, and H. V. Demr, "Phonon-Assisted Exciton Transfer into Silicon Using Nanoemitters: The Role of Phonons and Temperature Effects in Förster Resonance Energy Transfer", *ACS Nano*, vol. 7, no. 12, pp. 10 492–10 501, 2013. doi: 10.1021/nn404627p.

10. M'Saad, Hichem, *The Role of Surface and Bulk Perfection in the Processing and Performance of Silicon,* Thesis (Ph.D.) – Massachusetts Institute of Technology, Dept. of Materials Science and Engineering, 1994.

11. N. S. Patel, C. Monmeyran, A. Agarwal, and L. C. Kimerling, "Point defect states in Sb-doped germanium," *J. Appl. Phys.*, vol. 118, no. 15, p. 155702, Oct. 2015.

12. G. L. Miller, D. a. H. Robinson, and J. D. Wiley, "Contactless measurement of semiconductor conductivity by radio frequency-free-carrier power absorption", *Review of Scientific Instruments*, vol. 47, no. 7, pp. 799–805, Jul. 1, 1976. doi: 10.1063/1.1134756.
13. Saleh, Bahaa E. A., and Malvin Carl. Teich. *Fundamentals of photonics*. Hoboken, NJ: Wiley-Interscience, 2009. Print.

14. George, Steven M. "Atomic Layer Deposition: An Overview." *Chemical Reviews* 110.1 (2010): 111-31. Web.

15. Akselrod, Gleb M., Parag B. Deotare, Nicholas J. Thompson, Jiye Lee, William A. Tisdale, Marc A. Baldo, Vinod M. Menon, and Vladimir Bulović. "Visualization of exciton transport in ordered and disordered molecular solids." *Nature Communications* 5 (2014): n. pag. Web.